

Atomic self-organization emerging from a tunable quadratures coupling

Jingtao Fan,^{1,2} Gang Chen,^{1,2,3,*} and Suotang Jia^{1,2}

¹*State Key Laboratory of Quantum Optics and Quantum Optics Devices,
Institute of Laser Spectroscopy, Shanxi University, Taiyuan 030006, China*

²*Collaborative Innovation Center of Extreme Optics, Shanxi University, Taiyuan 030006, China*

³*Collaborative Innovation Center of Light Manipulations and Applications,
Shandong Normal University, Jinan 250358, China*

The recent experimental observation of dissipation-induced structural instability provides new opportunities for exploring the competition mechanism between stationary and nonstationary dynamics [Science **366**, 1496 (2019)]. In that study, two orthogonal quadratures of cavity field are coupled to two different Zeeman states of a spinor Bose-Einstein condensate (BEC). Here we propose a novel scheme to couple two density-wave degrees of freedom of a BEC to two quadratures of the cavity field. Being drastically different from previous studies, the light-matter quadratures coupling in our model are endowed with a tunable coupling angle. Apart from the uniform and self-organized phases, we unravel a dynamically unstable state induced by the cavity dissipation. Interestingly, the dissipation defines a particular coupling angle, across which the instabilities disappear. Moreover, at this critical coupling angle, one of the two atomic density waves can be independently excited without affecting one another. It is also found that our system can be mapped into a reduced three-level model under the commonly used low-excitation-mode approximation. However, the effectiveness of this approximation is shown to be broken by the dissipation nature for some special system parameters, hinting a possibility that the low-excitation-mode approximation is insufficient in capturing some dissipation-sensitive physics. Our work enriches the quantum simulation toolbox in the cavity-quantum-electrodynamics system and broadens the frontiers of light-matter interaction.

I. INTRODUCTION

Dissipative quantum many-body system lies at the heart of diverse branches of physics such as statistical mechanics, condensed matter physics, and quantum optics [1]. Compared to its equilibrium analog, a system exposed to dissipation is even harder to be understood due to the somewhat uncontrolled environment couplings. Fortunately, with the rapid improvement of both experimental and theoretical techniques, lots of exciting progress in this realm have been made of late [2–20]. It has been shown that the interplay between coherent and dissipative dynamics can lead to a vast kinds of novel phenomena. Examples include nonequilibrium transition [2–12], interaction-mediated laser cooling [13, 14], topological effects [15], dynamical new universality classes [16–18], and multistability of quantum spins [19, 20]. Among various realizations of the dissipative system, the coherently driven atomic gases inside optical cavities emerges as a uniquely promising route [21–51]. On the one hand, photons leaking from the cavity not only provide a convenient way to access the the atomic state, but also open a controlled channel for the collective dissipative dynamics [52–59]. On the other hand, the scattered cavity photons feed back on the atomic degrees of freedom and effectively impose a dynamic potential [29–33], which favors a unitary evolution of atoms. The competition between the coherent and dissipative processes in this composite system are fairly responsible for interesting nonequilib-

rium collective dynamics and exotic steady states.

Recently, plenty of noticeable effects induced by the driven-dissipative nature of the atom-cavity system have been uncovered both experimentally [57–66] and theoretically [67–74]. The light-matter interaction considered by these studies has been, however, mostly limited to the coupling between an atomic density mode and a single quadrature of cavity fields, which loses potential physics rooted in the cooperative interplay among multiple light quadratures. Actually, the combined action of the two orthogonal quadratures may have major impacts on spin systems [75, 76]. For example, it has been predicted that the simultaneous coupling between quantum spins and the two orthogonal quadratures of a radiation field can lead to anomalous multicritical points [19]. Along the same research direction, some judicious experiments impose this type of coupling on two different Zeeman states of a spinor BEC [56, 77], demonstrating that the competition between coherent and dissipative processes can even trigger a structural instability [56]. This progress further advances a series of relevant theoretical works [78–80]. Nevertheless, given that the quadrature operator of light is characterized by a phase factor representing a rotation angle (dubbed coupling angle) in the phase space [81], these researches focus only on the orthogonal light-atom coupling case where the coupling angle is frozen to $\pi/2$, leaving the interaction mechanism arising from a more generic coupling angle largely unexplored. This encourages us to raise the following fundamental questions: (i) what new physics may emerge from the light-matter interaction if the involved quadratures of radiation field can be tuned via the coupling angle? (ii) what is the role of dissipation in such a system?

*chengang971@163.com

In this paper, we address these questions by studying a driven-dissipative BEC-cavity system. We propose an experimental scheme, where two density-wave degrees of freedom of the BEC couple to two quadratures of the cavity field. In contrast to previous proposals, here the two quadratures of the cavity field carry a coupling angle θ , which, together with their respective pump strengths, are feasibly tunable. By allowing the participation of nonorthogonal quadratures of light, this setting broadens the frontiers of conventional light-matter interaction. Our main results are as follows.

(i) For a closed system without dissipation, the two atomic density modes can be excited respectively by varying the pump strength and coupling angle. This gives rise to four possible steady-state phases, all of which are shown to be stable against fluctuations.

(ii) The incorporation of cavity dissipation leads to a novel unstable region, which qualitatively changes the phase diagram of the closed system. By adiabatically eliminating the cavity field, we obtain an analytical expression determining the boundary between the stable and unstable regions. The unstable region is maximized if the two quadratures are orthogonal, whereas a coupling angle deviating from this orthogonal case tends to stabilize the phase diagram. Interestingly, the dissipation defines a particular coupling angle θ_c , across which the instabilities completely disappears. More importantly, when the coupling angle equals θ_c , one of the two density modes can be independently excited without affecting one another, which reproduces the character of its equilibrium version with $\theta = \pi/2$. Going beyond the adiabatic elimination, we find the whole regions of normal phase becomes unstable. The instabilities coming from the nonadiabaticity, however, turns out to be negligible for typical parameters in the current experiments.

(iii) Under the commonly used low-excitation-mode approximation [27–29], the system can be mapped into a paradigmatic quantum-optics model, which describes a single-mode quantized light field interacting with three-level atoms through different transition channels. However, we show the dissipation nature could break the effectiveness of the three-level model for some parameters, hinting that the low-excitation-mode approximation may be questionable in capturing some dissipation-sensitive physics.

The work is organized as follows. In Sec. II, we describe the proposed system configuration and present the Hamiltonian. In Sec. III, we present the mean-field approach used in calculating the phase diagrams. In Sec. IV, we calculate the phase diagram for the closed system. In Sec. V, we carry out a stability analysis and characterize the effects of dissipation on the system. In Sec. VI, we show the steady-state phase diagram for the driven-dissipative system. In Sec. VII, we explore the impacts of the nonadiabaticity of the cavity field on the phase diagram by including the dynamics of the cavity fluctuations. In Sec. VIII, we map the system into a reduced three-level model by the three-mode approxi-

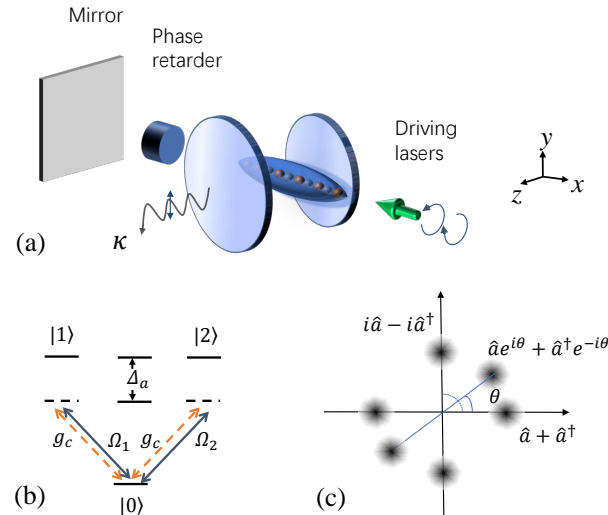


FIG. 1: (a) Schematic illustration of the considered setup. A quasi-1D BEC is illuminated by a pair of orthogonally-polarized lasers that is backreflected by a mirror. The phase retarder sitting inbetween the mirror and the BEC produces polarization-dependent optical lengths for traversed laser lights, and thereby imparts an additional phase shift between the two backforward propagating light fields. (b) The atomic level scheme. The atoms are simultaneously driven by the cavity field (red dashed arrows) and the counterpropagating lasers (blue solid arrows). (c) Sketch of the field distribution in the phase space responsible for different cavity quadratures.

mation. We discuss the experimental implementation in Sec. IX, and summarize in Sec. X.

II. SYSTEM

As illustrated in Fig. 1(a), we consider a BEC prepared inside an optical cavity and driven by a pair of orthogonally-polarized lasers. The BEC is assumed to be a cigar shape (with length L) elongated along the x direction, which we take as the quantization axis. The two driving lasers, which are frequency degenerate but with independently tunable phases and amplitudes, copropagate along the x direction, forming a generic elliptically-polarized single beam before impinging on the atoms. After propagating through the BEC, this laser beam is then backreflected from a mirror, and traverses the BEC a second time. A polarization-sensitive phase retarder is placed inbetween the mirror and the BEC, imparting an additional phase shift between the two orthogonally-polarized backforward propagating fields. The incident lasers with the same polarizations couple the electronic ground state $|0\rangle$ of the atoms to two excited states $|1\rangle$ and $|2\rangle$ with Rabi frequencies Ω_1 and Ω_2 , respectively. The optical cavity, whose main axis is arranged perpendicular to the long axis of the BEC, singles out a specific quantization mode and typically enhances its interaction

with the atoms. The selected cavity mode simultaneously mediates the transitions $|0\rangle \longleftrightarrow |1\rangle$ and $|0\rangle \longleftrightarrow |2\rangle$ with coupling strength g_c [see Fig. 1(b)]. The cavity frequency ω_c is closed to that of the driving lasers ω_p , both of which are detuned far below the atomic transition frequency ω_a , i.e., $|\Delta_a| \equiv |\omega_p - \omega_a| \gg \Omega_{1,2}$. Adiabatically eliminating the excited states yields the Hamiltonian of the atom-cavity system

$$\hat{\mathcal{H}} = -\hbar \left(\Delta_c - \frac{g_c^2}{\Delta_a} \right) \hat{a}^\dagger \hat{a} + \int \hat{\psi}^\dagger(x) \hat{H}_a \hat{\psi}(x) dx, \quad (1)$$

with g_c^2/Δ_a as a constant optical potential per photon and the cavity detuning $\Delta_c = \omega_p - \omega_c$. The single particle Hamiltonian density is obtained as (see Appendix A for details)

$$\begin{aligned} \hat{H}_a = & -\frac{\hbar^2}{2m} \frac{\partial^2}{\partial x^2} + \hbar\eta_1 \cos(kx)(\hat{a} + \hat{a}^\dagger) \\ & + \hbar\eta_2 \sin(kx)(\hat{a}e^{i\theta} + \hat{a}^\dagger e^{-i\theta}) \\ & + \hbar V_1 \cos^2(kx) + \hbar V_2 \sin^2(kx). \end{aligned} \quad (2)$$

Here, $\hat{\psi}(x)$ is the matter wave field operator for the atomic ground state and \hat{a} is the annihilation operator of the cavity photon. We have introduced the driving-field-induced lattice depth $V_{1(2)} = \Omega_{1(2)}^2/\Delta_a$ and the effective cavity pump strength $\eta_{1(2)} = \Omega_{1(2)} g_c s / \Delta_a$, with the constant s coming from transverse integrals (see Appendix A). The photon loss with rate κ is included in the model via a master equation of the form $\partial_t \hat{\rho} = -i/\hbar [\hat{\mathcal{H}}, \hat{\rho}] + \hat{\mathcal{L}}\hat{\rho}$, where the Lindblad operator acts as $\hat{\mathcal{L}}\hat{\rho} = \kappa(2\hat{a}\hat{p}\hat{a}^\dagger - \hat{a}^\dagger\hat{a}\hat{p} - \hat{p}\hat{a}^\dagger\hat{a})$. In the following discussion, we neglect the last two terms of Eq. (2) by assuming $V_1 \approx V_2$ for simplicity. This assumption does not affect the main results of this paper.

As a noteworthy feature of the system, two out-of-phase atomic density waves, $\cos(kx)$ and $\sin(kx)$, are respectively coupled to two quadratures of the cavity field. The relative coordinate of the two cavity quadratures is controlled by a coupling angle θ , which quantifies a rotation of the field distribution in phase space [see Fig. 1(c) for illustration]. We emphasize that the pump strength and coupling angle are both competing parameters that determine the interplay between the two atomic density waves.

In general, the Hamiltonian (2) possesses a \mathbb{Z}_2 symmetry representing its invariance under the transformation $\hat{a} \rightarrow -\hat{a}$ and $x \rightarrow x + \lambda/2$. Of particular interest is the special case $\theta = \pi/2$, where the original \mathbb{Z}_2 symmetry turns into a $\mathbb{Z}_2^{(1)} \otimes \mathbb{Z}_2^{(2)}$ double discrete symmetry [75], which is composed of two other transformations

$$\begin{aligned} (\hat{a} + \hat{a}^\dagger, i\hat{a} - i\hat{a}^\dagger, x) & \xrightarrow{\mathcal{T}_1} (-\hat{a} - \hat{a}^\dagger, i\hat{a} - i\hat{a}^\dagger, -x + \lambda/2), \\ (\hat{a} + \hat{a}^\dagger, i\hat{a} - i\hat{a}^\dagger, x) & \xrightarrow{\mathcal{T}_2} (\hat{a} + \hat{a}^\dagger, -i\hat{a} + i\hat{a}^\dagger, -x). \end{aligned}$$

This symmetry is further enhanced if both $\theta = \pi/2$ and $\eta_1 = \eta_2$ are satisfied. In this case, the Hamiltonian is

invariant under the simultaneous spatial transformation $x \rightarrow x + X$ and the cavity-phase rotation $\hat{a} \rightarrow \hat{a}e^{-ikX}$, which yields a continuous $U(1)$ symmetry associated with the freedom of an arbitrarily chosen displacement X . In the spirit of Landau's theory, it is anticipated that the aforementioned symmetries should be spontaneously broken by corresponding phase transitions. However, the dissipation nature plays a subtle role in the presented system, which prohibits the steady-state phase transitions associated with the enhanced $\mathbb{Z}_2^{(1)} \otimes \mathbb{Z}_2^{(2)}$ and $U(1)$ symmetries. This is because (i) the $\mathbb{Z}_2^{(1)} \otimes \mathbb{Z}_2^{(2)}$ symmetry owned by the Hamiltonian is explicitly broken by the Lindblad operator, and (ii) the dissipation induces extra phase shift for the cavity photons, preventing the arbitrariness of the value of X , which therefore makes the $U(1)$ symmetry breaking impossible. The physics demonstrating these points will be detailed in the subsequent sections.

It is worth noting that, moreover, fixing $\theta = \pi/2$ but keeping η_1 and η_2 as freely controlled parameters is equivalent to its dual case, namely setting $\eta_1 = \eta_2$ without any constraint on θ . To see this clearly, let us set $\theta = \pi/2$ and reparametrize the effective cavity pump strengths by $\eta_1 = \eta \cos(\varphi/2)$ and $\eta_2 = \eta \sin(\varphi/2)$. The single particle Hamiltonian (2) therefore reads

$$\begin{aligned} \hat{H}_a = & -\frac{\hbar^2}{2m} \frac{\partial^2}{\partial x^2} + \hbar\eta \cos(\varphi/2) \cos(kx)(\hat{a} + \hat{a}^\dagger) \\ & + \hbar\eta \sin(\varphi/2)(i\hat{a} - i\hat{a}^\dagger) \\ & + \hbar V_1 \cos^2(kx) + \hbar V_2 \sin^2(kx). \end{aligned} \quad (3)$$

Moving into a new gauge by using the transformations $a \rightarrow ae^{i\varphi/2}$ and $x \rightarrow x - \lambda/8$, the Hamiltonian (3) exactly reproduces the form of Eq. (2),

$$\begin{aligned} \hat{H}_a = & -\frac{\hbar^2}{2m} \frac{\partial^2}{\partial x^2} + \hbar\eta \cos(kx)(\hat{a} + \hat{a}^\dagger) \\ & + \hbar\eta \sin(kx)(\hat{a}e^{i\varphi} + \hat{a}^\dagger e^{-i\varphi}) \\ & + \hbar V_1 \cos^2(kx) + \hbar V_2 \sin^2(kx). \end{aligned} \quad (4)$$

where $\eta_1 = \eta_2 = \eta$ and φ plays the role of θ . In this sense, if setting $\theta = \pi/2$ (or equivalently $\eta_1 = \eta_2$), our model shares some similarities with those in Refs. [56, 77, 78]. However, as will be shown, letting both θ and $\eta_{1,2}$ to be controllable parameters, the proposed model accommodates more interesting physics which is completely out of the reach of other previous proposals.

III. MEAN-FIELD APPROACH

In the thermodynamic limit, it is a good approximation to neglect the quantum correlation between light and matter and thereby treat them as classical variables. At this mean-field level, the system is described by a set of coupled equations for the cavity field amplitude $\langle \hat{a}(t) \rangle = \alpha(t) = |\alpha(t)| e^{i\phi(t)}$, and atomic condensate wave function

$\langle \hat{\psi}(x, t) \rangle = \sqrt{N}\psi(x, t) = \sqrt{Nn(x, t)}e^{i\tau}$ (see Appendix B),

$$i\frac{\partial}{\partial t}\alpha = (-\delta_c - i\kappa)\alpha + N\eta_1\Theta_1 + N\eta_2e^{-i\theta}\Theta_2, \quad (5)$$

$$i\frac{\partial}{\partial t}\psi = \left[-\frac{\hbar}{2m}\frac{\partial^2}{\partial x^2} + \eta_1 \cos(kx)(\alpha + \alpha^*) + \eta_2 \sin(kx)(\alpha e^{i\theta} + \alpha^* e^{-i\theta}) \right] \psi, \quad (6)$$

where N is the atom number, $\delta_c = \Delta_c - g_c^2/\Delta_a$ is the effective cavity detuning, and $\Theta_1 \equiv \int n(x) \cos(kx)dx$ and $\Theta_2 \equiv \int n(x) \sin(kx)dx$ respectively represent the occupations of the two out-of-phase density modes, which we identify as order parameters. The last two terms of Eq. (5) account for the cavity photon generation rates. Note that these two terms respectively come from the coherent scattering between the pump field and different atomic density mode, giving rise to distinct cavity photons. That is, the term proportional to η_1 excites only one quadrature of the cavity photons, whereas the other term contributes another quadrature which is characterized by a rotation of θ in the phase space. It should be noticed that these two quadratures of cavity field are basically nonorthogonal to each other except for $\theta = \pi/2$. The backactions of the photon scattering on the atomic matter wave are reflected on the terms proportional to $\cos(kx)$ and $\sin(kx)$ in Eq. (6). These terms generate a space-dependent optical potential which has a periodicity of λ .

As we are interested in the steady state of the system, we self-consistently solve Eqs. (5)-(6) by setting $\partial_t\alpha = 0$ and $i\partial_t\psi = \mu\psi$, where μ is the chemical potential of the condensate. It is clear that, if either one of the pump strengths η_1 and η_2 is set zero, the system reduces to the conventional transversely pumped BEC inside a cavity, whose physics has been widely investigated both theoretically [50–52] and experimentally [28–30]. In that case, by increasing the pump strength, a “superradiant phase transition” from a state with no photon inside the cavity into a state with the appearance of macroscopic cavity field, takes place. Richer phenomena emerge if both η_1 and η_2 are turned on. To understand these aspects comprehensively, we first present the result of closed system ($\kappa = 0$) and then inspect the impacts of finite photon dissipation.

IV. PHASE DIAGRAM FOR THE CLOSED SYSTEM

Figure 2 plots the phase diagram for the dissipationless ($\kappa = 0$) BEC-cavity system as a function of η_1 and η_2 . We first pay attention to the orthogonal coupling case, $\theta = \pi/2$ [see Fig. 2(a)], considering its particular symmetry. According to the values of η_1 and η_2 , the steady state is identified as four different quantum phases. Specifically, when both η_1 and η_2 are below a critical value $\eta_c = \sqrt{-\delta_c\omega_R/2N}$ (see Sec. V for the derivation), the cavity

mode is empty and the density of the condensate keeps uniform with $\Theta_1 = \Theta_2 = 0$, corresponding to the normal phase (NP). For $\eta_1 > \eta_c$ and $\eta_1 > \eta_2$, the BEC is driven into a self-organized density-wave state characterized by $\Theta_1 \neq 0$ and $\Theta_2 = 0$, which we denote as density wave I (DW I). Similarly, for $\eta_2 > \eta_c$ and $\eta_2 > \eta_1$, we achieve another density-wave state characterized by $\Theta_1 = 0$ and $\Theta_2 \neq 0$, which is termed density wave II (DW II). Here, DW I and DW II are essentially symmetry-broken state which respectively breaks the $\mathbb{Z}_2^{(1)}$ and $\mathbb{Z}_2^{(2)}$ symmetries. A more interesting case is $\eta_1 = \eta_2 > \eta_c$, where both two density modes are excited with $\Theta_1 \neq 0$ and $\Theta_2 \neq 0$, and we name this phase as mixed density wave (MDW). Since in this case, the cavity-field phase ϕ can spontaneously take any arbitrary value between 0 to 2π , the continuous $U(1)$ symmetry is broken.

As phase diagrams for any $\theta \neq \pi/2$ resemble each other (they distinguish themselves solely by minor modifications of the phase boundaries), we take $\theta = \pi/5$ as a representative example. As shown in Fig. 2(b), the NP is located within a zone encircled by a smooth phase boundary. For points $\{\eta_1, \eta_2\}$ outside this zone, we have $\Theta_1 \neq 0$ and $\Theta_2 \neq 0$, corresponding to the MDW. This picture persists for any coupling angle with $\theta \neq \pi/2$, implying that a discrepancy from $\theta = \pi/2$ introduces a coupling between the two density modes $\cos(kx)$ and $\sin(kx)$, and thus excludes the emergence of either DW I or DW II. In other words, the only allowed phase transition in this case is the one from the NP to the MDW.

By further investigating the discontinuities of the order parameters, we find the transition from the DW I to the DW II is of first order while the transitions between any other two phases are of second order.

V. STABILITY ANALYSIS

We start to investigate the more appealing driven-dissipative properties by incorporating a nonzero photon-loss rate κ into the model. Since any potential dissipation-induced instability can not be fully captured by solely solving the equations of motion, we prefer to carry out a stability analysis around the trivial solution ($\psi \equiv 1/\sqrt{L}$, $\alpha = 0$) before presenting the final phase diagram. To this end, we work on the dispersive limit, saying $(|\delta_c|, \kappa) \gg (\omega_R, \sqrt{N}\eta_{1,2})$ with $\omega_R = \hbar k^2/2m$ being the recoil frequency, which allows us to adiabatically eliminate the cavity field by equating the field amplitude α with its steady-state value $\alpha = (N\eta_1\Theta_1 + N\eta_2e^{-i\theta}\Theta_2)/(\delta_c + i\kappa) = R \exp(i\chi)(N\eta_1\Theta_1 + N\eta_2e^{-i\theta}\Theta_2)$. Note here $R = 1/\sqrt{\delta_c^2 + \kappa^2}$ and we have introduced the dissipation-induced phase shift $\chi = \arctan(\kappa/\delta_c)$ [56]. Under this adiabatic approximation, the coupled equa-

tions of motion reduce to a single one,

$$i\frac{\partial}{\partial t}\psi = \left\{ -\frac{\hbar}{2m}\frac{\partial^2}{\partial x^2} + \frac{2\hbar N\eta_1 \cos(kx)}{\delta_c^2 + \kappa^2} [\cos(\theta)\delta_c\eta_2 \langle \sin(kx) \rangle - \sin(\theta)\kappa\eta_2 \langle \sin(kx) \rangle + \delta_c\eta_1 \langle \cos(kx) \rangle] + \frac{2\hbar N\eta_2 \sin(kx)}{\delta_c^2 + \kappa^2} [\cos(\theta)\delta_c\eta_1 \langle \cos(kx) \rangle - \sin(\theta)\kappa\eta_1 \langle \cos(kx) \rangle + \delta_c\eta_2 \langle \sin(kx) \rangle] \right\} \psi, \quad (7)$$

where the symbol $\langle \cdots \rangle$ stands for the average over single-atom wave function, $\langle \psi | \cdots | \psi \rangle$. We then effect a small fluctuation from the stationary state (ψ_0): $\psi(x, t) = e^{-i\mu t/\hbar} [\psi_0(x) + \delta\psi(x, t)]$. Inserting this ansate into Eq. (7) and neglecting higher-order correlations, we obtain an equation linearized in $\delta\psi$,

$$\begin{aligned} i\frac{\partial}{\partial t}\delta\psi = & \left(-\frac{\hbar}{2m}\frac{\partial^2}{\partial x^2} - \frac{\mu}{\hbar} \right) \delta\psi + \frac{2\eta_1 \cos(kx)}{\delta_c^2 + \kappa^2} [\cos(\theta)\delta_c\eta_2 (\langle \delta\psi | \sin(kx) | \psi_0 \rangle + \langle \psi_0 | \sin(kx) | \delta\psi \rangle) - \sin(\theta)\kappa\eta_2 (\langle \delta\psi | \sin(kx) | \psi_0 \rangle + \langle \psi_0 | \sin(kx) | \delta\psi \rangle) + \delta_c\eta_1 (\langle \delta\psi | \cos(kx) | \psi_0 \rangle + \langle \psi_0 | \cos(kx) | \delta\psi \rangle) + \sin(\theta)\kappa\eta_1 (\langle \delta\psi | \cos(kx) | \psi_0 \rangle + \langle \psi_0 | \cos(kx) | \delta\psi \rangle) + \sin(\theta)\kappa\eta_2 (\langle \delta\psi | \sin(kx) | \psi_0 \rangle + \langle \psi_0 | \sin(kx) | \delta\psi \rangle)] \psi_0 \\ & + \frac{2\eta_1 \cos(kx)}{\delta_c^2 + \kappa^2} [\cos(\theta)\delta_c\eta_2 (\langle \delta\psi | \cos(kx) | \psi_0 \rangle + \langle \psi_0 | \cos(kx) | \delta\psi \rangle) + \sin(\theta)\kappa\eta_2 (\langle \delta\psi | \cos(kx) | \psi_0 \rangle + \langle \psi_0 | \cos(kx) | \delta\psi \rangle) + \sin(\theta)\kappa\eta_1 (\langle \delta\psi | \sin(kx) | \psi_0 \rangle + \langle \psi_0 | \sin(kx) | \delta\psi \rangle)] \psi_0. \end{aligned} \quad (8)$$

We further assume the fluctuation evolves in the form: $\delta\psi(x, t) = \delta\psi_+(x)e^{-i\omega t/\hbar} + \delta\psi_-^*(x)e^{i\omega^* t/\hbar}$, where $\omega = \nu - i\gamma$ is a complex parameter with ν and γ being the oscillation frequency and damping rate, respectively. Equation (8) is then recast in a matrix form, $\omega\mathbf{v} = M\mathbf{v}$, where $\mathbf{v} = (\delta\psi_+, \delta\psi_-)^T$ and

$$M = \begin{pmatrix} H_0/\hbar + \Pi_* & \Pi \\ -\Pi & -H_0/\hbar - \Pi_* \end{pmatrix}, \quad (9)$$

with $\Pi = \Xi_+ \mathcal{I}_+ + \Xi_- \mathcal{I}_-$ and $\Pi_* = \Xi_+ \mathcal{I}_{*+} + \Xi_- \mathcal{I}_{*-}$. In the matrix (9), $H_0 = -\hbar^2/2m\partial_x^2 - \mu$, $\Xi_+ = N[2\eta_1^2 \cos(kx)\delta_c\psi_0 + 2\eta_1\eta_2 \sin(kx)(\cos(\theta)\delta_c + \sin(\theta)\kappa)\psi_0]/(\delta_c^2 + \kappa^2)$, $\Xi_- = N[2\eta_2^2 \sin(kx)\delta_c\psi_0 + 2\eta_1\eta_2 \cos(kx)(\cos(\theta)\delta_c - \sin(\theta)\kappa)\psi_0]/(\delta_c^2 + \kappa^2)$, and \mathcal{I}_\pm ($\mathcal{I}_{\pm*}$) is an integral operator defined as $\mathcal{I}_\pm \xi = \int_0^\lambda \psi_0(x) \cos(kx - \pi/4 \pm \pi/4)\xi dx/\lambda$ ($\mathcal{I}_{\pm*} \xi = \int_0^\lambda \psi_0^*(x) \cos(kx - \pi/4 \pm \pi/4)\xi dx/\lambda$). Assuming uniform condensate distribution ($\psi_0 \equiv 1/\sqrt{L}$), the definition of the integral operators \mathcal{I}_\pm and $\mathcal{I}_{\pm*}$ indicates that only the Fourier components $\cos(kx)$ and $\sin(kx)$ couple to the fluctuations, which motivates us to search solutions in the form

$$\begin{aligned} \delta\psi_+ &= \frac{1}{2} [(\delta\psi_+^1 + \delta\psi_-^1) \cos(kx) + (\delta\psi_+^2 + \delta\psi_-^2) \sin(kx)], \\ \delta\psi_- &= \frac{1}{2} [(\delta\psi_+^1 - \delta\psi_-^1) \cos(kx) + (\delta\psi_+^2 - \delta\psi_-^2) \sin(kx)]. \end{aligned}$$

Under the basis of $\mathbf{v}' = (\delta\psi_+^1, \delta\psi_-^1, \delta\psi_+^2, \delta\psi_-^2)^T$, it is straightforward to write the dynamical matrix as

$$\mathcal{M} = \begin{pmatrix} 0 & -\omega_R & 0 & 0 \\ \omega_R + \zeta_1 & 0 & \varpi_+ & 0 \\ 0 & 0 & 0 & -\omega_R \\ \varpi_- & 0 & \omega_R + \zeta_2 & 0 \end{pmatrix}, \quad (10)$$

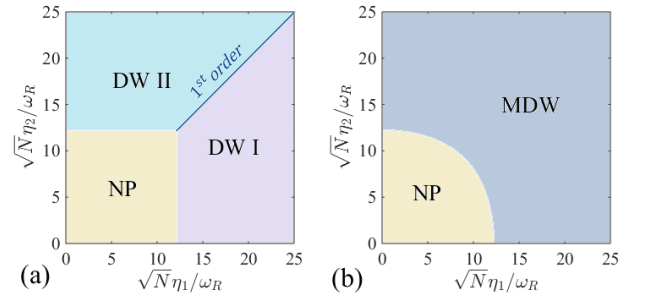


FIG. 2: Steady-state phase diagrams for closed systems ($\kappa = 0$) with (a) $\theta = \pi/2$ and (b) $\theta = \pi/5$, when $\delta_c/\omega_R = -300$.

where $\varpi_+ = 2N\eta_1\eta_2R \cos(\theta + \chi)$, $\varpi_- = 2N\eta_1\eta_2R \cos(\theta - \chi)$, $\zeta_1 = 2N\eta_1^2R \cos(\chi)$, and $\zeta_2 = 2N\eta_2^2R \cos(\chi)$. Note that for later convenience, the entries are intentionally parametrized in terms of χ and R instead of the more familiar ones κ and δ_c . Here, ζ_1 and ζ_2 act as energy shifts, whereas ϖ_+ and ϖ_- denote the cavity-mediated couplings between the two density modes. From the definition of ϖ_\pm , it is clear that the couplings are generated by the nonorthogonal coupling angle θ ($\neq \pi/2$) and the photon dissipation χ ($\neq 0$). That said, the role of dissipation is even more particular since it makes the two couplings asymmetric ($\varpi_+ \neq \varpi_-$) and even own opposite signs ($\varpi_+ \varpi_- < 0$), hinting potential dissipation-induced instabilities, as will be described below.

By solving the characteristic equation $\text{Det}(\mathcal{M} - \omega I_{4 \times 4}) = 0$, the spectrum of \mathcal{M} is readily obtained as

$$\omega = \pm \sqrt{\omega_0\omega_R \pm \frac{\omega_R}{2} \sqrt{4\varpi_+\varpi_- + (\zeta_+ - \zeta_-)^2}} \quad (11)$$

with $\omega_0 = \omega_R + (\zeta_+ + \zeta_-)/2$. The zero frequency ($\omega = 0$) solution of Eq. (11) yields the threshold pump strengths

above which the uniform distributed atomic gases self-organize into density waves. Especially for $\kappa = 0$ and $\theta = \pi/2$, the two pump strengths decouple and we get a simple critical value $\eta_c = \sqrt{-\delta_c \omega_R}/2N$. A state becomes dynamically unstable if ω acquires both a positive imaginary part and a nonzero real part. By inspecting the expression of Eq. (11), the relation satisfying this requirement is found to be $4\varpi_+ \varpi_- + (\zeta_+ - \zeta_-)^2 < 0$, which, after a substitution of system parameters, results in the following simple form,

$$\sin^2(\varphi) > \frac{\cos^2(\chi)}{\sin^2(\theta)}, \quad (12)$$

with $\varphi = 2 \arctan(\eta_2/\eta_1)$ as we have defined in Sec. II. Notice that for this case, the imaginary part of eigenvalues always come in pairs constituted by negative and positive branches, which represent damping and amplification, respectively [see Fig. 3(a)]. It is the appearance of the positive branch, namely the amplified excitation, that renders the NP unstable. The instability is characterized by the loss of stationary steady state. In fact, a state which falls into the unstable regime responds to initial small fluctuations by undamped limit-cycle oscillations [56, 78, 79].

It can be found from Eq. (12) that, for a closed system ($\chi = 0$), we have $\cos^2(\chi)/\sin^2(\theta) \equiv 1/\sin^2(\theta) \geq 1$, which invalidates the inequality in Eq. (12) all the time. This implies that the dissipation plays the key role in the appearance of the instability, which is in contrast to some standard cavity-BEC systems [48–51]. There, the impacts of dissipation are qualitatively minor since only the phase transition point is altered without major modification of the phase diagram. Another crucial knowledge we can infer is that the unstable regime in the phase diagram is feasibly controlled by the coupling angle θ . Actually, tuning θ such that $\sin^2(\theta) < \cos^2(\chi)$, the instability completely disappears, meaning the whole phase diagram is fully stabilized irrespective of η_1 and η_2 . The equality, $\sin^2(\theta) = \cos^2(\chi)$, defines a critical point separating a fully stable regime and a regime with possible instability [see Fig. 4(a) for example]. Conversely, the unstable region is maximally enlarged when $\theta = \pi/2$, which is nothing but the orthogonal coupling case realized in Refs. [56, 77]. From this point of view, embedding a tunable coupling angle in the light-matter interaction, our proposal offers new possibilities to either enhance or weaken the dissipation-induced instability in a controlled manner.

VI. STEADY-STATE QUANTUM PHASES FOR THE DRIVEN-DISSIPATIVE SYSTEM

It is the right stage to explore the quantum phases systematically. Figure 5 depicts the steady-state phase diagrams for several representative coupling angles (More phase diagrams and their comparison with the case of

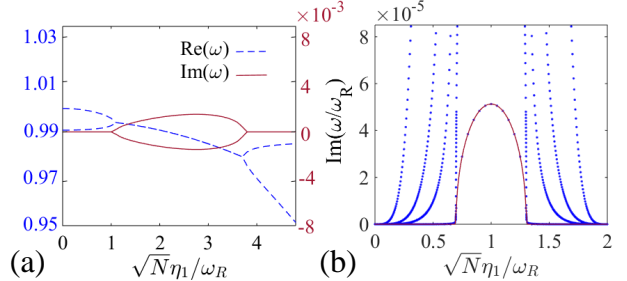


FIG. 3: (a) The real and imaginary part of the eigenvalues ω as a function of λ_1 for $\lambda_2/\omega_R = 2$, $\kappa/\omega_R = 200$, and $\delta_c/\omega_R = -300$. The results are obtained from Eq. (11). (b) The positive branch of the imaginary part of the eigenvalues ω (blue dots), along the transverse cut line, $\sqrt{N}\eta_2 = 2\omega_R - \sqrt{N}\eta_1$, depicted by red dotted line in Fig. 5(a). The results are obtained by diagonalizing the 6×6 dynamical matrix including cavity field fluctuations, for $\kappa/\omega_R = 5, 15, 50, 1000, 6000$ and $\delta_c/\omega_R = -1.5\kappa$. It can be seen that as the adiabatic limit is approached, the eigenvalues reduce to the results given by Eq. (11) (red solid lines).

closed system are attributed to Appendix C). We first focus on the orthogonal coupling case $\theta = \pi/2$. As shown in Fig. 5(a), the phase diagram is dramatically distinct from its equilibrium analog [see Fig. 2(a)]. An immediate observation is that the DW I and DW II predicted in Fig. 2(a) are mixed into a MDW due to the dissipative coupling. Moreover, the expected $U(1)$ symmetry-broken phase transition for $\eta_1 = \eta_2$ vanishes, and a considerably large region of dynamical instability (UST), enclosed by the critical curves defined by $\sin^2(\varphi) = \cos^2(\chi)$ (the blue dashed lines), emerges. As an additional inference, the equal-coupling case (i.e., $\eta_1 = \eta_2$) is sensitive to the dissipation so much so that any infinitely small κ leads to an instability.

The physics behind this can be well understood in a semi-classical picture. Treating quantum operators classically, we express the total single-particle energy as $E = -(\hbar^2/2m)\partial_x^2 + \mathcal{E}(x)$, where the self-consistent potential is given by

$$\mathcal{E}(x) = 2|\alpha|\eta_1 \cos(\phi) \cos(kx) - 2|\alpha|\eta_2 \sin(\phi) \sin(kx).$$

The onset of the self-organization is triggered by the periodicity of $\mathcal{E}(x)$, attracting more atoms to its minima where the equation $\partial_x \mathcal{E} = 0$ applies. This links the position coordinate with the cavity phase via

$$\tan(kx) = -\tan\left(\frac{\varphi}{2}\right) \tan(\phi). \quad (13)$$

On the other hand, the steady-state solution of the cavity amplitude reads $\alpha = NR e^{i\chi}[\eta_1 \cos(kx) - i\eta_2 \sin(kx)]$, producing

$$\tan(\phi) = \frac{\sin(\chi) - \cos(\chi) \tan(\varphi/2) \tan(kx)}{\cos(\chi) + \sin(\chi) \tan(\varphi/2) \tan(kx)}. \quad (14)$$

The existence of a solution for Eqs. (13) and (14) requires $\sin(\varphi) > \cos(\chi)$, which agrees with the result ob-

tained from the stability analysis. This picture also explains the absence of the $U(1)$ symmetry breaking for the case $\eta_1 = \eta_2$ (i.e., $\tan(\varphi/2) = 1$), since the dissipation-induced phase shift χ imposes extra constraint on the degree of freedom of ϕ through Eq. (14), which makes it frozen to specific value instead of picking up a random number from 0 to 2π .

Along this reasoning, it is expected that phase diagrams for other coupling angles should be qualitatively similar, saying the self-organized phase cannot be anything but the MDW [see Fig. 5(b) for example]. However, an intriguing phenomenon occurs when situating θ at the critical points described by $\sin^2(\theta) = \cos^2(\chi)$ (i.e., $\theta = \theta_c = \pm\chi \pm \pi/2$), as shown in Figs. 5(c) and 5(d). Considering the duality of Figs. 5(c) and 5(d), let us take $\theta = -\chi \pm \pi/2$ as an example. In this case, the phase diagram exactly recovers the skeleton of that in Fig. 2(a) where a closed system with $\theta = \pi/2$ operates. That is to say, the whole phase diagram is divided into three different regions, $\{\eta_1 \leq \tilde{\eta}_c, \eta_2 \leq \tilde{\eta}_c\}$, $\{\eta_1 > \tilde{\eta}_c, \eta_1 > \eta_2\}$, and $\{\eta_2 > \tilde{\eta}_c, \eta_2 > \eta_1\}$ with a redefined critical pump strength $\tilde{\eta}_c = \eta_c / \sin(\theta)$. Nevertheless, the major difference lies in the region $(\eta_2 > \tilde{\eta}_c, \eta_2 > \eta_1)$ where the MDW supersedes the DW II, and the first order transition presented in Fig. 2(a) becomes second order here. As complements, Figs. 4(a) and 4(b) show phase diagrams in the $\theta - \varphi$ plane for different pump strength η ($= \eta_1 = \eta_2$), from which the particularity of θ_c becomes clearer. These results look a bit counterintuitive, since both the nonorthogonal coupling and the cavity dissipation are apt to mix the two density modes. Our finding shows that the dissipation defines a particular coupling angle $\theta_c = \pm\chi \pm \pi/2$, in which the two mixing elements cooperate and somehow counteract each other.

Let us give a description for this exotic behavior. Observing only the Fourier components $\cos(kx)$ and $\sin(kx)$ of a fluctuation of the condensate wave function can excite a nonzero cavity field, we construct a trial initial wave function $\psi(x, 0) = \sqrt{1/L} + \epsilon_1 \sqrt{2/L} \cos(kx) + \epsilon_2 \sqrt{2/L} \sin(kx)$, with $|\epsilon_{1,2}| \ll 1$ [51]. Propagating $\psi(x, 0)$ by one iteration step of the imaginary time $\Delta\tau$ ($\tau = it$), we have $\psi(x, \Delta\tau) = \sqrt{1/L} + \delta\psi(x, \Delta\tau)$, where

$$\begin{aligned} \delta\psi(x, \Delta\tau) &= \{\epsilon_1 - [2NR \cos(\chi - \theta) \eta_1 \eta_2 \epsilon_2 + \omega_R \epsilon_1 \\ &\quad + 2NR \cos(\chi) \eta_1^2 \epsilon_1] \Delta\tau\} \sqrt{\frac{2}{L}} \cos(kx) \\ &\quad + \{\epsilon_2 - [2NR \cos(\chi + \theta) \eta_1 \eta_2 \epsilon_1 + \omega_R \epsilon_2 \\ &\quad + 2NR \cos(\chi) \eta_2^2 \epsilon_2] \Delta\tau\} \sqrt{\frac{2}{L}} \sin(kx). \end{aligned} \quad (15)$$

Under the basis of $\mathbf{v}'' = (\sqrt{2/L} \cos(kx), \sqrt{2/L} \sin(kx))$, Eq. (15) can be formulated in the matrix form, $\delta\psi(x, \Delta\tau) = (\delta\psi_1(x, \Delta\tau), \delta\psi_2(x, \Delta\tau))^T = \Gamma(\epsilon_1, \epsilon_2)^T$, where

$$\Gamma = \begin{pmatrix} 1 - \mathcal{D}_1 \Delta\tau & \mathcal{N}_- \Delta\tau \\ \mathcal{N}_+ \Delta\tau & 1 - \mathcal{D}_2 \Delta\tau \end{pmatrix}, \quad (16)$$

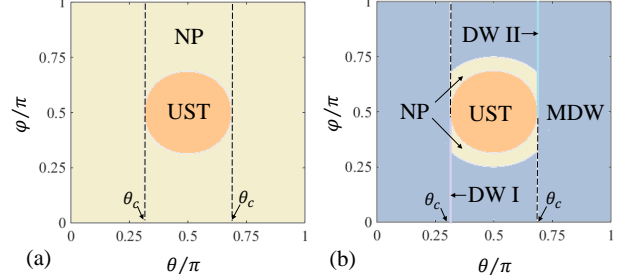


FIG. 4: Steady-state phase diagrams in the rescaled parameter space $\{\theta/\pi, \varphi/\pi\}$ for (a) $\sqrt{N}\eta_1/\omega_R = \sqrt{N}\eta_2/\omega_R = 10$ and (b) $\sqrt{N}\eta_1/\omega_R = \sqrt{N}\eta_2/\omega_R = 30$, when $\kappa/\omega_R = 200$ and $\delta_c/\omega_R = -300$. Region UST represents dynamically unstable phase, and the black dashed lines are defined by $\sin^2(\theta) = \cos^2(\chi)$, which determines the critical coupling angle θ_c .

with $\mathcal{D}_{1,2} = 2NR \cos(\chi) \eta_{1,2}^2 + \omega_R$ and $\mathcal{N}_\pm = -2NR \cos(\chi \pm \theta) \eta_1 \eta_2$. Inserting $\theta = -\chi + \pi/2$ into Γ and diagonalizing it, we get two eigenvalues $\Omega_1 = 1 - [2NR \cos(\chi) \eta_1^2 + \omega_R] \Delta\tau$ and $\Omega_2 = 1 - [2NR \cos(\chi) \eta_2^2 + \omega_R] \Delta\tau$, whose eigenvectors respectively reads $v_1 = (1, 0)^T$ and $v_2 = (-2\eta_1 \eta_2 \sin(\chi) / (\eta_1^2 - \eta_2^2), 1)^T$. Utilizing $\Omega_{1,2}$ and $v_{1,2}$, it is straightforward to obtain the wave function at $n\Delta\tau$,

$$\begin{aligned} \psi(x, n\Delta\tau) &= \sqrt{\frac{1}{L}} + \epsilon_2 \sqrt{\frac{2}{L}} [\sin(kx) \\ &\quad - \frac{2\eta_1 \eta_2 \sin(\chi)}{\eta_1^2 - \eta_2^2} \cos(kx)] \Omega_2^n \\ &\quad + \epsilon'_1 \sqrt{\frac{2}{L}} \cos(kx) \Omega_1^n, \end{aligned} \quad (17)$$

where $\epsilon'_1 = \epsilon_1 + 2\eta_1 \eta_2 \sin(\chi) / (\eta_1^2 - \eta_2^2) \epsilon_2$ and n can be any integer number. In Eq. (17), $\Omega_{1,2} < 1$ ($\Omega_{1,2} > 1$) represents decay (amplification) of corresponding modes, leading to the normal (self-organized) state in the long-time limit. Notice that the second line of Eq. (17) involves a term proportional to $\sin(kx) - 2\eta_1 \eta_2 \sin(\chi) / (\eta_1^2 - \eta_2^2) \cos(kx)$, it thus becomes evident that for $\eta_1 > \tilde{\eta}_c$ and $\eta_2 < \tilde{\eta}_c$ (namely, $\Omega_1 > 1$ and $\Omega_2 < 1$), only the cosine-like density wave $\propto \cos(kx)$ emerges (DW I), while for $\eta_2 > \tilde{\eta}_c$ and $\eta_1 < \tilde{\eta}_c$ (namely, $\Omega_1 < 1$ and $\Omega_2 > 1$), both two density waves are simultaneously excited (MDW). We emphasize that the above derivation is mainly based on a perturbation assumption, which works only around weak excitation regime, it should therefore not be strange that the present framework is not able to precisely predict the phase boundary between DW I and MDW.

For completeness, we put diagrams of the order parameters Θ_1 and Θ_1 , from which one obtain the phase diagrams of Figs. 2 and 5, in Appendix D.

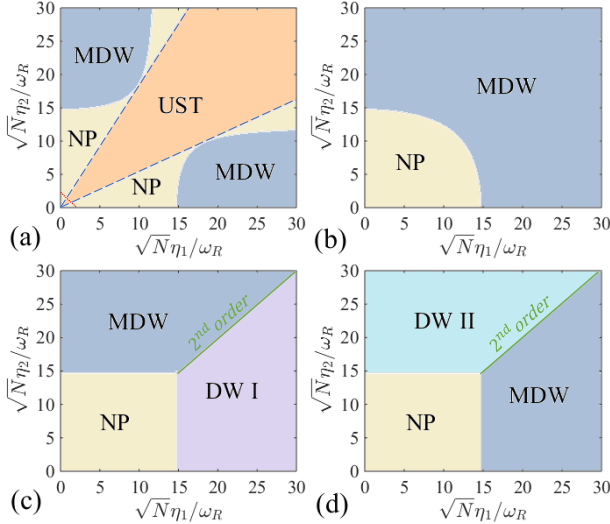


FIG. 5: Steady-state phase diagrams for the dissipative system, determined by the equations of motion (5-6) and a stability analysis, for varying coupling angles with (a) $\theta = \pi/2$, (b) $\theta = \pi/5$, (c) $\theta = -\chi + \pi/2 \approx 4.12$ and (d) $\theta = \chi + \pi/2 \approx -0.98$, when $\kappa/\omega_R = 200$ and $\delta_c/\omega_R = -300$. In (a), the blue dashed lines are defined by $\sin^2(\varphi) = \cos^2(\chi)$.

VII. BEYOND ADIABATIC ELIMINATION

Up to now, the discussion is restricted to the adiabatic limit where fluctuations of the cavity amplitude is omitted. We now go beyond the adiabatic approximation by including the dynamics of the cavity fluctuations $\delta\alpha$ and $\delta\alpha^*$ (see Appendix E). By doing this, we get a 6×6 dynamical matrix whose spectrum can not be expressed analytically. The numerical diagonalization of this matrix suggests that, the nonadiabaticity exert no influence on the self-organized phase but makes the NP unstable for all $\theta \neq 0, \pm\pi$. This arises from the observation that a nonzero positive imaginary part of the eigenvalues appears throughout the NP except for $\theta = 0, \pm\pi$. Figure 3(b) depicts the imaginary part of the these eigenvalues for some different δ_c and κ . We find that approaching the adiabatic limit ($|\delta_c|, \kappa \gg (\omega_R, \sqrt{N}\eta_{1,2})$), the results reduce to that given by Eq. (11).

VIII. THREE-MODE APPROXIMATION FOR THE BEC

Following the commonly used two-mode approximation [27–29], the matter field in our model can be spanned by minimally three Fourier-modes within the single recoil scattering limit,

$$\hat{\psi}(x) = \sqrt{\frac{1}{L}}\hat{c}_0 + \sqrt{\frac{2}{L}}\hat{c}_1 \cos(kx) + \sqrt{\frac{2}{L}}\hat{c}_2 \sin(kx), \quad (18)$$

where \hat{c}_0 , \hat{c}_1 , and \hat{c}_2 are bosonic annihilation operators for corresponding modes. It is more convenient to introduce

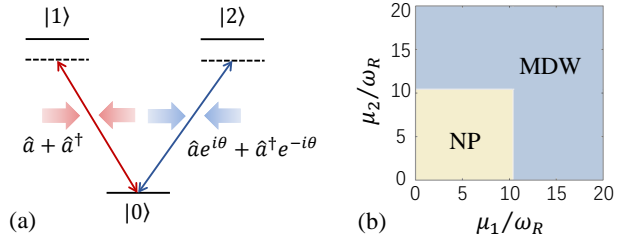


FIG. 6: (a) Three-level atoms interact with different quadratures of a single-mode quantized light field via transition channels $|0\rangle \longleftrightarrow |1\rangle$ and $|0\rangle \longleftrightarrow |2\rangle$, respectively. (b) Phase diagram for the effective model under three-mode approximation. The parameters are the same as those in Fig. 5(c).

the collective three-level operator $\hat{\Xi}_{ij} = \sum_{k=1}^N |i\rangle_k \langle j|_k$ with atomic states $\{|0\rangle_k, |1\rangle_k, |2\rangle_k\}$ ($k = 1, 2, \dots, N$). The operators $\hat{\Xi}_{ij}$ fulfill the $U(3)$ algebra commutation relations $[\hat{\Xi}_{ij}, \hat{\Xi}_{kl}] = \delta_{jk}\hat{\Xi}_{il} - \delta_{il}\hat{\Xi}_{kj}$. By invoking a generalized-Schwinger representation [82], $\hat{\Xi}_{ij} = \hat{c}_i^\dagger \hat{c}_j$ ($i, j = 0, 1, 2$), the Hamiltonian (1) in the three-mode subspace reads

$$\begin{aligned} \hat{H} = & -\hbar\delta_c\hat{a}^\dagger\hat{a} - \hbar\omega_R\hat{\Xi}_{00} + \frac{\hbar\mu_1}{\sqrt{N}}(\hat{\Xi}_{01} + \hat{\Xi}_{10})(\hat{a} + \hat{a}^\dagger) \\ & + \frac{\hbar\mu_2}{\sqrt{N}}(\hat{\Xi}_{02} + \hat{\Xi}_{20})(\hat{a}e^{i\theta} + \hat{a}^\dagger e^{-i\theta}), \end{aligned} \quad (19)$$

with the collective coupling strength $\mu_{1,2} = \eta_{1,2}\sqrt{2N}/2$. It is easy to check that the symmetry property here follows that in Hamiltonian (1). Especially, when $\mu_1 = \mu_2$ and $\theta = \pi/2$, the emergent $U(1)$ symmetry is characterized by a conserved quantity $\hat{\mathcal{C}} = \hat{a}^\dagger\hat{a} + i(\hat{\Xi}_{12} - \hat{\Xi}_{21})$, satisfying $[\hat{\mathcal{C}}, \hat{H}] = 0$. The effective Hamiltonian (19) describes a single-mode quantized light field interacting with three-level atoms, whose transition channels, $|0\rangle \longleftrightarrow |1\rangle$ and $|0\rangle \longleftrightarrow |2\rangle$, are coupled by different quadratures of light [see Fig. 6(a)].

The quantum phases for this model are classified by the expectation values of $\hat{\Xi}_{11}$ and $\hat{\Xi}_{22}$, whose roles are the same as those of Θ_1 and Θ_2 , respectively. Similarly, the phase diagram is straightforwardly obtained by exploiting the steady state of the equations of motion, $i\hbar\partial_t \langle \hat{\Xi}_{ij} \rangle = \langle [\hat{\Xi}_{ij}, \hat{H}] \rangle$ and $i\hbar\partial_t \langle \hat{a} \rangle = \langle [\hat{a}, \hat{H}] \rangle - i\hbar\kappa \langle \hat{a} \rangle$ (see Appendix F for details). While for most parameters we are interested in, the solutions are in accordance with the results obtained by directly solving Eqs. (5)-(6), a remarkable exception appears when tuning the coupling angle to the critical value $\theta_c = \pm\chi \pm \pi/2$. In this case, the three-level model predicts only two possible phases: NP and MDW, as shown in Fig. 6(b). This sharply contrasts with Figs. 5(c) and 5(d), which are plotted based on the solutions for Eqs. (5)-(6). As a matter of fact, provided the photon dissipation is incorporated, the three-level model always excludes the emergence of DW I and DW II. This finding provides an interesting example where the effectiveness of the three-mode approximation is radically

broken by the dissipation nature. It is thus a hint that the effective model under low-excitation-mode approximation may be insufficient in capturing certain physics when the dissipation starts to play a role. We leave the exploration of its microscopic origin to the future work.

IX. EXPERIMENTAL CONSIDERATION

In experiment, the two driving lasers can be respectively chosen as left- and right-circularly polarized. Accordingly, the atomic internal ground and excited states are hyperfine Zeeman states with magnetic levels $m = 0$ and $m \pm 1$, respectively. Given this, a promising candidate for the phase retarder is the Faraday rotator [83], which can impart arbitrary phase difference between the two backreflected circularly-polarized lasers. Since the coupling angle θ is acquired just from the phase retarder, it can be feasibly controlled by simply varying the magnetic field in the Faraday rotator. Moreover, the realization of the cosinelike and sinelike density coupling in the Hamiltonian (2) can be easily achieved by locking the phase difference of the two incident lasers to be $\pi/2$ (see Appendix A). While the experiment technique to directly distinguish the two density patterns $\cos(kx)$ and $\sin(kx)$ has been developed [60, 61], a more convenient way is to exploit the one-to-one correspondence between the cavity phase ϕ and the atomic density wave order parameters $\Theta_{1,2}$. In recognition of this, the goal to identify different density waves is mapped to detecting the cavity phase, which can be readily accomplished by using a heterodyne detection system analyzing the light field leaking from the cavity [55–57, 84].

X. CONCLUSIONS

In summary, we have proposed an experimental scheme, where two density-wave degrees of freedom of the BEC couple to two quadratures of the cavity field. Being drastically different from previous studies, here the coupling angle between the two quadratures is feasibly tunable, leading to new physics emerging from nonorthogonal quadratures coupling between light and matter. The cavity dissipation plays a decisive role in determining the steady-state phase diagram. For one thing, it induces a novel unstable region above the normal phase. For the other, it defines a particular coupling angle, across which the system exhibits some properties resembling its equilibrium analog. While additional antidampings may be generated by the nonadiabaticity of the cavity field, which renders the normal phase unstable, it turns out to be negligibly small for typical parameters in the current experiments. Moreover, for some special parameters, the commonly used low-excitation-mode approximation is shown to be questionable for our model due to the dissipation nature of the system.

Acknowledgments

This work is supported partly by the National Key R&D Program of China under Grant No. 2017YFA0304203; the NSFC under Grants No. 11674200 and No. 11804204; and 1331KSC.

Appendix A: Effective Hamiltonian

In this section, we provide the detailed derivation of Hamiltonian (1) in the main text. We start by considering the coupling of internal states of a single atom, as illustrated in Fig. 1(b) in the main text. The Hamiltonian can be decomposed as $\hat{H} = \hat{H}_0 + \hat{H}_I + \hat{H}_I^*$, where

$$\hat{H}_0 = \omega_c \hat{a}^\dagger \hat{a} + \sum_{j=1,2} \omega_j |j\rangle \langle j| + \frac{\hat{\mathbf{p}}^2}{2m} + V_R(\mathbf{r}), \quad (A1)$$

$$\hat{H}_I = -\frac{1}{2} \sum_{j=1,2} \left(\overleftarrow{\Omega}_j(x) e^{-i\omega_p t} |0\rangle \langle j| + g_c \hat{a} |0\rangle \langle j| + \text{H.c.} \right), \quad (A2)$$

$$\hat{H}_I^* = -\frac{1}{2} \sum_{j=1,2} \left(\overrightarrow{\Omega}_j(x) e^{-i\omega_p t} |0\rangle \langle j| + g_c \hat{a} |0\rangle \langle j| + \text{H.c.} \right), \quad (A3)$$

with the Rabi frequencies $\overleftarrow{\Omega}_j(x) = \Omega_j \exp[i(kx + \vartheta_j + \theta_j)]$ and $\overrightarrow{\Omega}_j(x) = \Omega_j \exp[-i(kx + \vartheta_j - \theta_j)]$. Note that \hat{H}_0 is the free Hamiltonian and \hat{H}_I (\hat{H}_I^*) represents the light-matter interaction contributed by the incident (backreflected) pumping lasers. In the Hamiltonians (A1)-(A3), $\hat{\mathbf{p}}^2/2m$ and $V_R(\mathbf{r})$ are the kinetic energy and transverse trapping potential respectively, and ω_j denotes the eigenfrequency of the atomic state $|j\rangle$ ($j = 1, 2$). The field operator \hat{a} describes the annihilation of a cavity photon with the frequency ω_c . The transitions $|0\rangle \leftrightarrow |1\rangle$ and $|0\rangle \leftrightarrow |2\rangle$ are respectively driven by two orthogonally-polarized pumping lasers with the Rabi amplitudes Ω_1 and Ω_2 . H.c. denotes the Hermitian conjugation. Since the BEC is arranged to be orthogonal to the cavity axis, the atom-cavity coupling g_c is space independent. We emphasize that the phase of the incident (backreflecting) laser mediating the transition $|0\rangle \leftrightarrow |j\rangle$ is given by $\vartheta_j + \theta_j$ ($\vartheta_j - \theta_j$). Therefore, the phase shift imparted by the phase retarder for the corresponding transition is $2\theta_j$.

We introduce a time-dependent unitary transformation, $\hat{U}(t) = \exp[i(\sum_{\sigma=1,2} |\sigma\rangle \langle \sigma| + \hat{a}^\dagger \hat{a})\hbar\omega_p t]$, under

which the Hamiltonian \hat{H} becomes

$$\begin{aligned}\hat{H} = & -\Delta_c \hat{a}^\dagger \hat{a} + \frac{\hat{\mathbf{p}}^2}{2m} + V_R(\mathbf{r}) \\ & - \sum_{j=1,2} \left(\Delta |j\rangle \langle j| + \frac{\overleftarrow{\Omega}_j(x)}{2} |0\rangle \langle j| \right. \\ & \left. + \frac{\overrightarrow{\Omega}_j(x)}{2} |0\rangle \langle j| + g \hat{a} |0\rangle \langle j| + \text{H.c.} \right), \quad (\text{A4})\end{aligned}$$

where $\Delta_c = \omega_p - \omega_c$ is the cavity detuning, $\Delta_a = \omega_p - \omega_1 \approx \omega_p - \omega_2$ denotes the detuning between pumping lasers and atomic eigenfrequencies. We work in the limit of large detuning $|\Delta_a| \gg \{|\Omega_{1,2}|, |g|, |\Delta_c|\}$, which allows us to adiabatically eliminate the excited states $|1\rangle$ and $|2\rangle$. The resulting effective Hamiltonian is given as

$$\begin{aligned}\hat{H} = & -\delta_c \hat{a}^\dagger \hat{a} + \frac{\hat{\mathbf{p}}^2}{2m} + V_R(\mathbf{r}) + \frac{\hbar \Omega_1 g_c}{\Delta_a} \cos(kx) (\hat{a} + \hat{a}^\dagger) \\ & + \frac{\hbar \Omega_2 g_c}{\Delta_a} \cos(kx + \vartheta) (\hat{a} e^{i\theta} + \hat{a}^\dagger e^{-i\theta}) \\ & + \frac{\hbar \Omega_1^2}{\Delta_a} \cos^2(kx) + \frac{\hbar \Omega_1^2}{\Delta_a} \cos^2(kx + \vartheta). \quad (\text{A5})\end{aligned}$$

where $\delta_c = \Delta_c - g_c^2/\Delta_a$. Note that in writing Hamiltonian (A5), a gauge with $\vartheta_2 = \vartheta$, $\theta_2 = \theta$, and $\vartheta_1 = \theta_1 = 0$ has been chosen. To describe the dynamics of N atoms, we extend the single particle Hamiltonian (A5) to the second-quantized form, i.e.,

$$\begin{aligned}\hat{\mathcal{H}} = & -\hbar \delta_c \hat{a}^\dagger \hat{a} + \int d^3 \mathbf{r} \hat{\Psi}^\dagger(\mathbf{r}) \left[\frac{\hat{\mathbf{p}}^2}{2m} + \hat{V}_R(\mathbf{r}) + \frac{\hbar \Omega_1 g_c}{\Delta_a} \right. \\ & \times \cos(kx) (\hat{a} + \hat{a}^\dagger) + \frac{\hbar \Omega_2 g_c}{\Delta_a} \cos(kx + \vartheta) \\ & \times (\hat{a} e^{i\theta} + \hat{a}^\dagger e^{-i\theta}) + \frac{\hbar \Omega_1^2}{\Delta_a} \cos^2(kx) \\ & \left. + \frac{\hbar \Omega_1^2}{\Delta_a} \cos^2(kx + \vartheta) \right] \hat{\Psi}(\mathbf{r}), \quad (\text{A6})\end{aligned}$$

where $\hat{\Psi}(\mathbf{r})$ denotes the field operator for annihilating an atom at position \mathbf{r} . We further assume $V_R(\mathbf{r})$ is strong enough so that the atomic motion in the transverse direction is frozen to the ground state. This enables us to integrate out the transverse degrees of freedom using $\hat{\Psi}(\mathbf{r}) = \sqrt{2/\pi\rho} \hat{\psi}(x) \exp[-(y^2 + z^2)/\rho^2]$, where ρ is a transverse characteristic length. The simplified one-dimensional Hamiltonian thus reads

$$\begin{aligned}\hat{\mathcal{H}} = & -\hbar \delta_c \hat{a}^\dagger \hat{a} + \int d^3 x \hat{\psi}^\dagger(x) \left[-\frac{\hbar^2}{2m} \frac{\partial^2}{\partial x^2} \right. \\ & + \hbar \eta_2 \cos(kx + \vartheta) (\hat{a} e^{i\theta} + \hat{a}^\dagger e^{-i\theta}) \\ & + \hbar \eta_1 \cos(kx) (\hat{a} + \hat{a}^\dagger) + \hbar V_1 \cos^2(kx) \\ & \left. + \hbar V_2 \cos^2(kx + \vartheta) \right] \hat{\psi}(x), \quad (\text{A7})\end{aligned}$$

where $V_{1,2} = \Omega_{1,2}^2/\Delta_a$ and $\eta_{1,2} = \Omega_{1,2} g_c s/\Delta_a$, with $s = \exp(-k^2 \rho^2/8)$. By setting $\vartheta = \pi/2$, Eq. (A7) reduces to Hamiltonian (1) in the main text.

Appendix B: Mean-field equations

The Heisenberg equations of the photon annihilation operator \hat{a} and the matter wave field operator $\hat{\psi}(x)$ is derived by using the Hamiltonian $\hat{\mathcal{H}}$,

$$i \frac{\partial}{\partial t} \hat{a} = \frac{1}{\hbar} [\hat{a}, \hat{\mathcal{H}}] = (-\hbar \delta_c - i\hbar \kappa) \hat{a} + \eta_1 \hat{\Theta}_1 + \eta_2 e^{-i\theta} \hat{\Theta}_2, \quad (\text{B1})$$

$$i \frac{\partial}{\partial t} \hat{\psi}(x) = \frac{1}{\hbar} [\hat{\psi}(x), \hat{\mathcal{H}}] = \frac{1}{\hbar} \hat{H}_a \hat{\psi}(x), \quad (\text{B2})$$

where $\hat{\Theta}_1 = \int d^3 x \hat{\psi}^\dagger(x) \cos(kx) \hat{\psi}(x)$ and $\hat{\Theta}_2 = \int d^3 x \hat{\psi}^\dagger(x) \sin(kx) \hat{\psi}(x)$. Note that we have added the cavity decay rate κ in Eq. (B1). Replacing the quantum field operators \hat{a} and $\hat{\psi}(x)$ by their averages $\langle \hat{a}(t) \rangle = \alpha(t) = |\alpha(t)| e^{i\phi(t)}$ and $\langle \hat{\psi}(x, t) \rangle = \sqrt{N} \psi(x, t) = \sqrt{N n(x, t)} e^{i\tau}$, respectively, we get the mean-field equations (5)-(6) in the main text.

Appendix C: More phase diagrams

As plotted in Fig. 7, we provide more phase diagrams to show the contrast between the dissipative (top panel) and dissipationless (bottom panel) systems.

Appendix D: Diagrams of the order parameters

Figure 8 shows the steady-state solutions of order parameters Θ_1 and Θ_2 with the same parameters as those in Figs. 2 and 5, obtained by numerically solving Eqs. (5)-(6). In these phase diagrams, Figs. 8(ai)-8(bi) correspond to Figs. 2(a) and 2(b) and Figs. 8(ci)-8(fi) correspond to Figs. 5(a)-5(d) with $i \in \{1, 2\}$, respectively. It should be noticed that, within the shaded area in Figs. 8(c1) and 8(c2), the system loses stationary steady-state solutions but features limit-cycle oscillations in the long-time limit.

Appendix E: Stability analysis beyond adiabatic elimination

We go beyond adiabatic elimination by incorporating the dynamics of the cavity fluctuations $\delta\alpha$ and $\delta\alpha^*$. Assuming $\psi(x, t) = e^{-i\mu t/\hbar} [\psi_0(x) + \delta\psi(x, t)]$ and $\alpha(t) = \alpha_0 + \delta\alpha$, where $\psi_0(x)$ and α_0 are the steady-state solution of Eqs. (5)-(6) in the main text. The equations of motion linearized in $\delta\psi$ and $\delta\alpha$ read

$$\begin{aligned}i\hbar \frac{\partial}{\partial t} \delta\psi_- = & \left(-\frac{\hbar^2}{2m} \frac{\partial^2}{\partial x^2} - \mu \right) \delta\psi \\ & + \psi_0 \eta_1 \cos(kx) (\delta\alpha + \delta\alpha^*) \\ & + \psi_0 \eta_2 \sin(kx) (\delta\alpha e^{i\theta} + \delta\alpha^* e^{-i\theta}), \quad (\text{E1})\end{aligned}$$

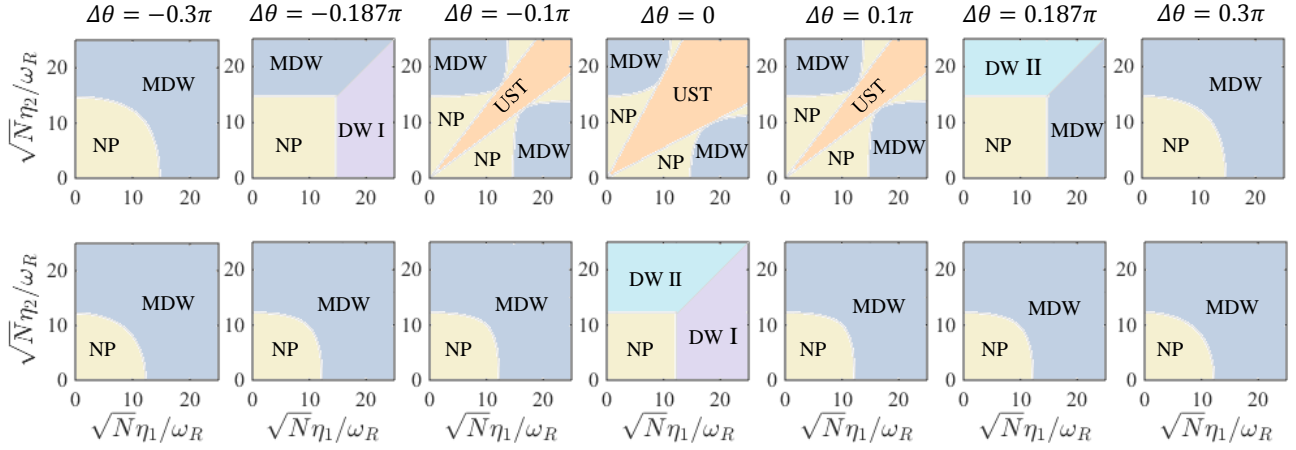


FIG. 7: Phase diagrams with $\delta_c/\omega_R = -300$ and different $\Delta\theta$, where $\Delta\theta = \theta - \pi/2$. The top and bottom panels correspond to $\kappa/\omega_R = 200$ and $\kappa/\omega_R = 0$, respectively.

$$\begin{aligned} i\hbar \frac{\partial}{\partial t} \delta\alpha &= N\eta_1 \int dx \cos(kx) (\psi_0^* \delta\psi + \psi_0 \delta\psi^*) \\ &+ N\psi_0 \eta_2 \int dx \cos(kx) (\psi_0^* \delta\psi + \psi_0 \delta\psi^*) e^{-i\theta} \\ &(-\hbar\delta_c - i\hbar\kappa) \delta\alpha. \end{aligned} \quad (\text{E2})$$

Along the strategy employed in Sec. V, we substitute the ansate $\delta\psi(x, t) = \delta\psi_+(x)e^{-i\omega t/\hbar} + \delta\psi_-(x)e^{-i\omega^* t/\hbar}$ and $\delta\alpha(t) = \delta\alpha_+ e^{-i\omega t/\hbar} + \delta\alpha_-^* e^{i\omega^* t/\hbar}$ into Eqs. (E1)-(E2) and obtain

$$\begin{aligned} \hbar\omega\delta\psi_+ &= \left(-\frac{\hbar^2}{2m} \frac{\partial^2}{\partial x^2} - \mu \right) \delta\psi_+ \\ &+ \psi_0 \eta_1 \cos(kx) (\delta\alpha_+ + \delta\alpha_-) \\ &+ \psi_0 \eta_2 \sin(kx) (\delta\alpha_+ e^{i\theta} + \delta\alpha_- e^{-i\theta}), \end{aligned} \quad (\text{E3})$$

$$\begin{aligned} \hbar\omega\delta\psi_- &= \left(\frac{\hbar^2}{2m} \frac{\partial^2}{\partial x^2} + \mu \right) \delta\psi_- \\ &- \psi_0 \eta_1 \cos(kx) (\delta\alpha_+ + \delta\alpha_-) \\ &- \psi_0 \eta_2 \sin(kx) (\delta\alpha_+ e^{i\theta} + \delta\alpha_- e^{-i\theta}), \end{aligned} \quad (\text{E4})$$

$$\begin{aligned} \hbar\omega\delta\alpha_+ &= N\eta_1 \int dx \cos(kx) (\psi_0^* \delta\psi_+ + \psi_0 \delta\psi_-) \\ &+ N\eta_2 \int dx \sin(kx) (\psi_0^* \delta\psi_+ + \psi_0 \delta\psi_-) e^{-i\theta} \\ &+ (-\hbar\delta_c + i\hbar\kappa) \delta\alpha_+, \end{aligned} \quad (\text{E5})$$

$$\begin{aligned} \hbar\omega\delta\alpha_- &= -N\psi_0 \eta_1 \int dx \cos(kx) (\psi_0^* \delta\psi_+ + \psi_0 \delta\psi_-) \\ &- N\eta_2 \int dx \sin(kx) (\psi_0^* \delta\psi_+ + \psi_0 \delta\psi_-) e^{-i\theta} \\ &+ (\hbar\delta_c - i\hbar\kappa) \delta\alpha_-. \end{aligned} \quad (\text{E6})$$

These equations can be recast in a matrix form $\omega\mathbf{f} = \mathcal{M}\mathbf{f}$, with $\mathbf{f} = (\delta\psi_+, \delta\psi_-, \delta\alpha_+, \delta\alpha_-)^T$, and

$$\mathcal{M} = \begin{pmatrix} H_k - \mu & 0 & \psi_0(K_1(x) + K_2(x)e^{i\theta}) & \psi_0(K_1(x) + K_2(x)e^{-i\theta}) \\ 0 & -H_k + \mu & -\psi_0(K_1(x) + K_2(x)e^{i\theta}) & -\psi_0(K_1(x) + K_2(x)e^{-i\theta}) \\ N(\eta_1 \mathcal{I}_{+*} + \eta_2 e^{-i\theta} \mathcal{I}_{-*}) & N(\eta_1 \mathcal{I}_+ + \eta_2 e^{-i\theta} \mathcal{I}_-) & -\delta_c + i\kappa & 0 \\ -N(\eta_1 \mathcal{I}_{+*} + \eta_2 e^{-i\theta} \mathcal{I}_{-*}) & -N(\eta_1 \mathcal{I}_+ + \eta_2 e^{-i\theta} \mathcal{I}_-) & 0 & \delta_c - i\kappa \end{pmatrix}, \quad (\text{E7})$$

where $K_1(x) = \eta_1 \cos(kx)$, $K_2(x) = \eta_2 \sin(kx)$ and $H_k = -(\hbar^2/2m) \partial_x^2$ is the kinetic energy.

Using the trivial solution ($\psi_0(x) = 1/\sqrt{L}$, $\alpha_0 = 0$),

and the ansates $\delta\psi_{\pm} = \delta\psi_{\pm}^{(1)} \cos(kx) + \delta\psi_{\pm}^{(2)} \sin(kx)$, the dynamical matrix takes the following 6×6 form,

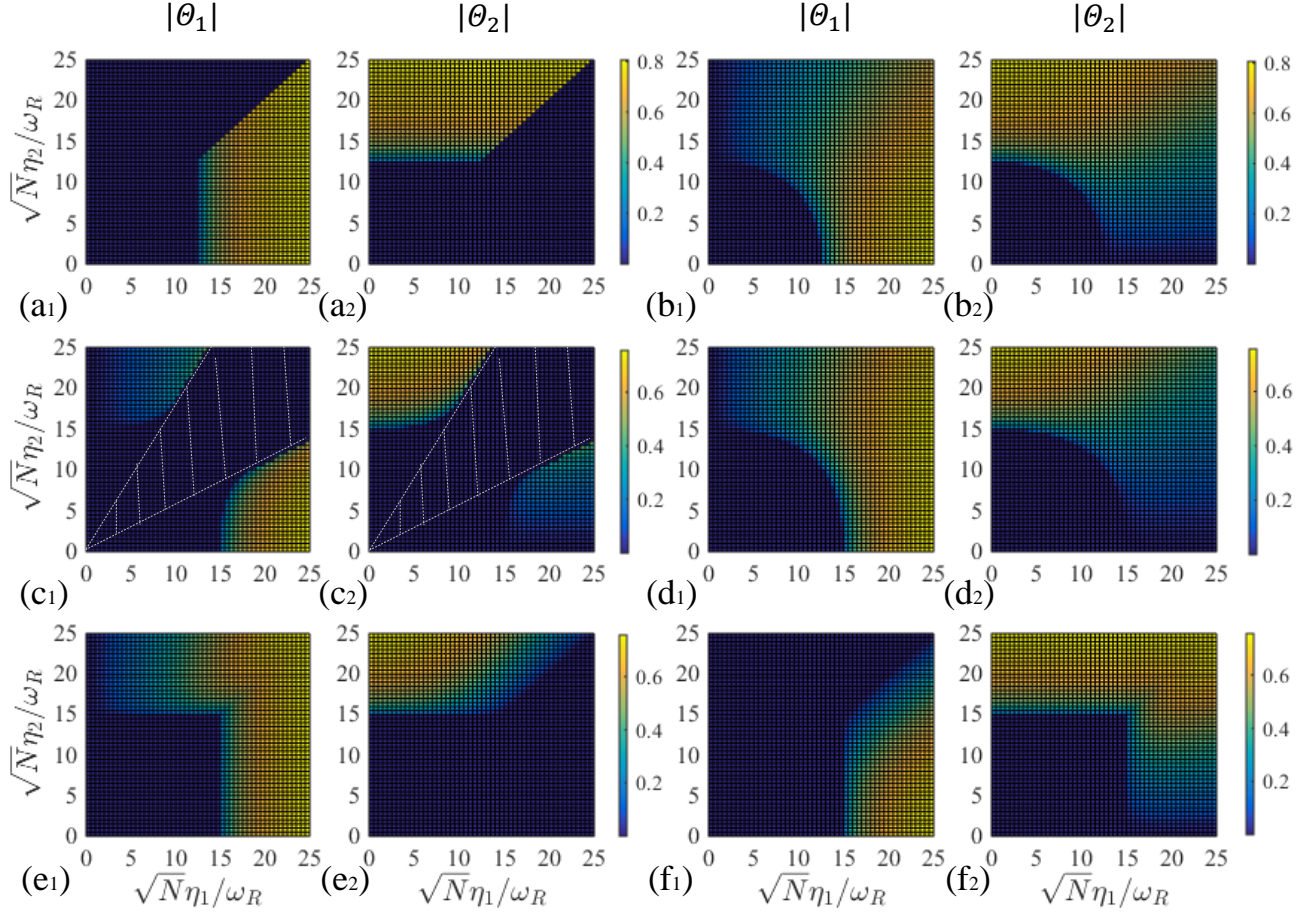


FIG. 8: Order parameters $|\Theta_1|$ and $|\Theta_2|$ for (a1)-(a2) $\kappa/\omega_R = 0$, $\theta = \pi/2$, (b1)-(b2) $\kappa/\omega_R = 0$, $\theta = \pi/5$, (c1)-(c2) $\kappa/\omega_R = 200$, $\theta = \pi/2$, (d1)-(d2) $\kappa/\omega_R = 200$, $\theta = \pi/5$, (e1)-(e2) $\kappa/\omega_R = 200$, $\theta = 4.12$, and (f1)-(f2) $\kappa/\omega_R = 200$, $\theta = -0.98$, with $\delta_c/\omega_R = -300$. The shaded areas in (c1) and (c2) indicate the absence of stationary steady-state solutions.

$$\tilde{\mathcal{M}} = \begin{pmatrix} \omega_R & 0 & 0 & 0 & \eta_1 & \eta_1 \\ 0 & -\omega_R & 0 & 0 & -\eta_1 & -\eta_1 \\ 0 & 0 & \omega_R & 0 & \eta_2 e^{i\theta} & \eta_2 e^{-i\theta} \\ 0 & 0 & 0 & -\omega_R & -\eta_2 e^{i\theta} & -\eta_2 e^{-i\theta} \\ N\eta_1/2 & N\eta_1/2 & N\eta_2 e^{-i\theta}/2 & N\eta_2 e^{-i\theta}/2 & -\delta_c + i\kappa & 0 \\ -N\eta_1/2 & -N\eta_1/2 & -N\eta_2 e^{i\theta}/2 & -N\eta_2 e^{i\theta}/2 & 0 & \delta_c - i\kappa \end{pmatrix}. \quad (\text{E8})$$

The eigenvalues ω of $\tilde{\mathcal{M}}$ are the solutions of the sixth-order characteristic equation $\text{Det}(\mathcal{M} - \omega I_{6 \times 6}) = 0$, namely the solutions of

Appendix F: Steady-state quantum phases for the effective three-level model

$$[(\delta_c\omega_R + 2N\eta_1^2)\omega_R + \delta_c\omega^2] [(\delta_c\omega_R + 2N\eta_2^2)\omega_R + \delta_c\omega^2] = (\omega + i\kappa)^2(\omega_R^2 - \omega^2)^2 + 4\omega_R^2 N^2 \eta_1^2 \eta_2^2 \cos^2(\theta). \quad (\text{E9})$$

In this section, we describe the methods in obtaining the phase diagram of the effective three-level model in more detail. Choosing the state $|0\rangle$ as a reference, we apply the generalized Holstein-Primakoff transformation

[85, 86] to rewrite the operators $\hat{\Xi}_{ij}$ as

$$\hat{\Xi}_{00} = N - \sum_{i=1,2} b_i^\dagger b_i, \quad (\text{F1})$$

$$\hat{\Xi}_{12} = b_1^\dagger b_2, \quad (\text{F2})$$

$$\hat{\Xi}_{s0} = b_s^\dagger \sqrt{N - \sum_{i=1,2} b_i^\dagger b_i} \quad (s = 1, 2), \quad (\text{F3})$$

where b_i^\dagger and b_i are bosonic operators. In order to construct a mean-field theory, the bosonic operators are assumed to be composed of their expectation value and a fluctuation operator, i.e.,

$$a = \alpha + \delta a, \quad b_1 = \beta_1 + \delta b_1, \quad b_2 = \beta_2 + \delta b_2, \quad (\text{F4})$$

where $\alpha = \langle a \rangle$, $\beta_1 = \langle b_1 \rangle$, and $\beta_2 = \langle b_2 \rangle$ are complex mean-field parameters. According to Eq. (F4), the operators $\hat{\Xi}_{ij}$ can be expanded as

$$\begin{aligned} \hat{\Xi}_{00} &= Nk - \beta_1 \delta b_1^\dagger - \beta_2 \delta b_2^\dagger - \beta_1^* \delta b_1 - \beta_2^* \delta b_2 + \mathcal{O}(2), \\ \hat{\Xi}_{12} &= \beta_1^* \beta_2 + \beta_2 \delta b_1^\dagger + \beta_1 \delta b_2^\dagger + \mathcal{O}(2), \\ \hat{\Xi}_{i0} &= \sqrt{Nk} \delta b_i^\dagger + \sqrt{k} \beta_i^* + \mathcal{O}(2) \quad (i = 1, 2), \\ \hat{\Xi}_{ii} &= |\beta_i|^2 + \beta_i \delta b_i^\dagger + \beta_i^* \delta b_i + \mathcal{O}(2) \quad (i = 1, 2). \end{aligned}$$

In terms of the mean-field parameters α and β_i ($i = 1, 2$), the semi-classical equations of motion, $i\hbar \partial_t \langle \hat{\Xi}_{ij} \rangle =$

$\langle [\hat{\Xi}_{ij}, \hat{\mathcal{H}}] \rangle$ and $i\hbar \partial_t \langle \hat{a} \rangle = \langle [\hat{a}, \hat{\mathcal{H}}] \rangle - i\hbar \kappa \langle \hat{a} \rangle$, are derived as

$$\begin{aligned} i \frac{\partial}{\partial t} \beta_1 &= -\omega_R \beta_1 - \frac{\mu_1 (\alpha + \alpha^*) (|\beta_1|^2 - N)}{\sqrt{k}} \\ &\quad - \frac{\mu_2 (\alpha e^{i\theta} + \alpha^* e^{-i\theta}) \beta_2^* \beta_1}{\sqrt{k}}, \end{aligned} \quad (\text{F5})$$

$$\begin{aligned} i \frac{\partial}{\partial t} \beta_2 &= -\omega_R \beta_2 - \frac{\mu_2 (\alpha + \alpha^*) (|\beta_2|^2 - N)}{\sqrt{k}} \\ &\quad - \frac{\mu_1 (\alpha e^{i\theta} + \alpha^* e^{-i\theta}) \beta_1^* \beta_2}{\sqrt{k}}, \end{aligned} \quad (\text{F6})$$

$$\begin{aligned} i \frac{\partial}{\partial t} \alpha &= (-\delta_c - i\kappa) \alpha + \mu_1 \sqrt{k} (\beta_1 + \beta_1^*) \\ &\quad + \mu_2 \sqrt{k} e^{-i\theta} (\beta_2 + \beta_2^*). \end{aligned} \quad (\text{F7})$$

Following the same manner we did in Sec. V of the main text, the stability of the steady-state solutions of Eqs. (F5)-(F7) are determined by analyzing the linearized fluctuation equations, $i\dot{\mathbf{f}}_T = \mathcal{M}_T \mathbf{f}_T$, with $\mathbf{f}_T = (\delta\psi_+, \delta\psi_-, \delta\alpha_+, \delta\alpha_-)^T$ and

$$\mathcal{M}_T = \begin{pmatrix} -\Delta - i\kappa & 0 & \mu_1 \sqrt{k} & \mu_2 \sqrt{k} e^{-i\theta} & \mu_2 \sqrt{k} e^{-i\theta} \\ 0 & \Delta + i\kappa & -\mu_1 \sqrt{k} & -\mu_2 \sqrt{k} e^{i\theta} & -\mu_2 \sqrt{k} e^{i\theta} \\ -B_1^*(-\theta) & -B_1^*(\theta) & \omega_R - \Lambda_1^* & -\mu_1 \beta_2^* \varrho(0) - \mu_2 \beta_1^* \varrho(\theta) & -\mu_1 \beta_2^* \varrho(0) \\ B_1(\theta) & B_1(-\theta) & 2\mu_1 \beta_1 \varrho(0) & \mu_1 \beta_2 \varrho(0) + \mu_2 \beta_1 \varrho(\theta) & \mu_1 \beta_2 \varrho(0) \\ -B_2^*(-\theta) & -B_2^*(\theta) & -\mu_2 \beta_1^* \varrho(\theta) & -\mu_1 \beta_2 \varrho(0) - \mu_2 \beta_1^* \varrho(\theta) & -2\mu_2 \beta_1^* \varrho(\theta) \\ B_2(\theta) & B_2(-\theta) & \mu_1 \beta_2^* \varrho(0) + \mu_2 \beta_1 \varrho(\theta) & \mu_2 \beta_1 \varrho(\theta) & -\omega_R + \Lambda_2 \end{pmatrix}. \quad (\text{F8})$$

Here $\varrho(\theta) = (\alpha \exp(i\theta) + \alpha^* \exp(-i\theta)) / \sqrt{k}$, $B_1(\theta) = [\mu_1 (|\beta_1|^2 - k) + \mu_2 \beta_1^* \beta_2 \exp(i\theta)] / \sqrt{k}$, $B_2(\theta) = [\mu_2 (|\beta_2|^2 - k) + \mu_1 \beta_2^* \beta_1 \exp(i\theta)] / \sqrt{k}$, $\Lambda_1 = 2\mu_1 \beta_1 \varrho(0) + \mu_2 \beta_2 \varrho(\theta)$, and $\Lambda_2 = \mu_1 \beta_1 \varrho(0) + 2\mu_2 \beta_2 \varrho(\theta)$. From Eqs. (F5)-(F8), the mean-field parameters characterizing different quantum phases can be uniquely determined.

The solutions in the case of $\theta = \pi/2$ and $\kappa = 0$ are summarized as follows. Firstly, for $(\mu_1, \mu_2) < \mu_c$, with $\mu_c = \sqrt{-\delta_c \omega_R} / 2 \equiv \eta_c \sqrt{2N} / 2$, both $\langle \hat{\Xi}_{11} \rangle$ and $\langle \hat{\Xi}_{22} \rangle$ vanish, which defines the NP. Secondly, for $\mu_1 > \mu_c$ and $\mu_1 > \mu_2$, we have $\langle \hat{\Xi}_{11} \rangle / N = (4\mu_1^2 + \delta_c \omega_R) / 8\mu_1^2$ and $\langle \hat{\Xi}_{22} \rangle / N = 0$. This means that the atoms start populating the state $|1\rangle$, which corresponds to the DW I. Thirdly, for $\mu_2 > \mu_c$ and $\mu_2 > \mu_1$, we obtain $\langle \hat{\Xi}_{22} \rangle / N = (4\mu_2^2 + \delta_c \omega_R) / 8\mu_2^2$

and $\langle \hat{\Xi}_{11} \rangle / N = 0$, indicating the state $|2\rangle$ is occupied. This corresponds to the DW II. Lastly, for $\mu_1 = \mu_2 > \mu_c$, the values of $\langle \hat{\Xi}_{11} \rangle$ and $\langle \hat{\Xi}_{22} \rangle$ are determined by the equation $\langle \hat{\Xi}_{11} \rangle / N + \langle \hat{\Xi}_{22} \rangle / N = (4\mu_{1,2}^2 + \delta_c \omega_R) / 8\mu_{1,2}^2$, signaling both $|1\rangle$ and $|2\rangle$ can be populated, and thus the MDW is realized.

Notice that analytical solutions for more generic parameters are not available. However, it can still be straightforwardly found that the mean-field parameters satisfying $\beta_1 \beta_2 = 0$ and $\beta_1 + \beta_2 \neq 0$ could by no means be a steady-state solution to Eqs. (F5)-(F7), except for the case of $\theta = \pi/2$ and $\kappa = 0$. This implies that, at least under the framework of three-mode approximation, the DW I and DW II can not exist for any other parameter

settings.

[1] U. Weiss, *Quantum Dissipative Systems*, Third Edition (World Scientific, 2008).

[2] J. Kasprzak, M. Richard, S. Kundermann, A. Baas, P. Jeambrun, J. M. J. Keeling, F. M. Marchetti, M. H. Szymaska, R. Andr, J. L. Staehli, *et. al.*, Bose–Einstein condensation of exciton polaritons, *Nature (London)* **443**, 409 (2006).

[3] N. Syassen, D. M. Bauer, M. Lettner, T. Volz, D. Dietze, J. J. García-Ripoll, J. I. Cirac, G. Rempe, and S. Dürr, Strong Dissipation Inhibits Losses and Induces Correlations in Cold Molecular Gases, *Science* **320**, 1329 (2008).

[4] A. Amo, D. Sanvitto, F. P. Laussy, D. Ballarini, E. d. Valle, M. D. Martin, A. Lematre, J. Bloch, D. N. Krizhanovskii, M. S. Skolnick, *et. al.*, Collective fluid dynamics of a polariton condensate in a semiconductor microcavity, *Nature (London)* **457**, 291 (2009).

[5] D. Nagy, G. Kóya, G. Szirmai, and P. Domokos, Dicke-Model Phase Transition in the Quantum Motion of a Bose-Einstein Condensate in an Optical Cavity, *Phys. Rev. Lett.* **104**, 130401 (2010).

[6] F. Brennecke, R. Mottl, K. Baumann, R. Landig, T. Donner, and T. Esslinger, Real-time observation of fluctuations at the driven-dissipative Dicke phase transition, *Proc. Natl. Acad. Sci. U.S.A.* **110**, 035302 (2013).

[7] G. Barontini, R. Labouvie, F. Stubenrauch, A. Vogler, V. Guarrera, and H. Ott, Controlling the Dynamics of an Open Many-Body Quantum System with Localized Dissipation, *Phys. Rev. Lett.* **110**, 035302 (2013).

[8] J. Klinder, H. Keßler, M. Wolke, L. Mathey, and A. Hemmerich, Dynamical phase transition in the open Dicke model, *Proc. Natl. Acad. Sci. U.S.A.* **112**, 3290 (2015).

[9] T. Fink, A. Schade, S. Höfing, C. Schneider, and A. Imamoglu, Signatures of a dissipative phase transition in photon correlation measurements, *Nat. Phys.* **14**, 365 (2018).

[10] T. Tomita, S. Nakajima, I. Danshita, Y. Takasu, and Y. Takahashi, Observation of the Mott insulator to superfluid crossover of a driven-dissipative Bose-Hubbard system, *Sci. Adv.* **3**, e1701513 (2017).

[11] S. Smale, P. He, B. A. Olsen, K. G. Jackson, H. Sharum, S. Trotzky, J. Marino, A. M. Rey, and J. H. Thywissen, Observation of a transition between dynamical phases in a quantum degenerate Fermi gas, *Sci. Adv.* **5**, eaax1568 (2019).

[12] J. T. Young, A. V. Gorshkov, M. Foss-Feig, and M. F. Maghrebi, Non-equilibrium fixed points of coupled Ising models, *Phys. Rev. X* **10**, 011039 (2020).

[13] S. D. Huber and H. P. Büchler, Dipole-Interaction-Mediated Laser Cooling of Polar Molecules to Ultracold Temperatures, *Phys. Rev. Lett.* **108**, 193006 (2012).

[14] B. Zhao, A. W. Glaetzle, G. Pupillo, and P. Zoller, Atomic Rydberg Reservoirs for Polar Molecules, *Phys. Rev. Lett.* **108**, 193007 (2012).

[15] S. Diehl, E. Rico, M. A. Baranov, and P. Zoller, Topology by Dissipation in Atomic Quantum Wires, *Nat. Phys.* **7**, 971 (2011).

[16] S. Diehl, A. Tomadin, A. Micheli, R. Fazio, and P. Zoller, Dynamical Phase Transitions and Instabilities in Open Atomic Many-Body Systems, *Phys. Rev. Lett.* **105**, 015702 (2010).

[17] D. Nagy, G. Szirmai, and P. Domokos, Critical exponent of a quantum-noise-driven phase transition: The open-system Dicke model, *Phys. Rev. A* **84**, 043637 (2011).

[18] L. M. Sieberer, S. D. Huber, E. Altman, and S. Diehl, Dynamical Critical Phenomena in Driven-Dissipative Systems, *Phys. Rev. Lett.* **110**, 195301 (2013).

[19] M. Soriente, T. Donner, R. Chitra, and O. Zilberberg, Dissipation-Induced Anomalous Multicritical Phenomena, *Phys. Rev. Lett.* **120**, 183603 (2018).

[20] H. Landa, M. Schiró, and G. Misguich, Multistability of Driven-Dissipative Quantum Spins, *Phys. Rev. Lett.* **124**, 043601 (2020).

[21] H. Ritsch, P. Demokos, F. Brennecke, and T. Esslinger, Cold atoms in cavity-generated dynamical optical potentials, *Rev. Mod. Phys.* **85**, 553 (2013).

[22] J. Fan, Z. Yang, Y. Zhang, J. Ma, G. Chen, and S. Jia, Hidden continuous symmetry and Nambu-Goldstone mode in a two-mode Dicke model, *Phys. Rev. A* **89**, 023812 (2014).

[23] Y. Feng, K. Zhang, J. Fan, F. Mei, G. Chen, and S. Jia, Superfluid-superradiant mixed phase of the interacting degenerate Fermi gas in an optical cavity, *SCIENCE CHINA: Physics, Mechanics & Astronomy*, **61**, 123011 (2018).

[24] X. Guan, J. Fan, X. Zhou, G. Chen, and S. Jia, Two-component lattice bosons with cavity-mediated long-range interaction, *Phys. Rev. A* **100**, 013617 (2019).

[25] S. C. Schuster, P. Wolf, S. Ostermann, S. Slama, and C. Zimmermann, Supersolid Properties of a Bose-Einstein Condensate in a Ring Resonator, *Phys. Rev. Lett.* **124**, 143602 (2020).

[26] J. Lénard, A. Morales, P. Zupancic, T. Donner, and T. Esslinger, Monitoring and manipulating Higgs and Goldstone modes in a supersolid quantum gas, *Science* **358**, 1415 (2017).

[27] J. Lénard, A. Morales, P. Zupancic, T. Esslinger, and T. Donner, Supersolid formation in a quantum gas breaking continuous translational symmetry, *Nature (London)* **543**, 87 (2017).

[28] K. Baumann, C. Guerlin, F. Brennecke, and T. Esslinger, Dicke quantum phase transition with a superfluid gas in an optical cavity, *Nature (London)* **464**, 1301 (2010).

[29] R. Mottl, F. Brennecke, K. Baumann, R. Landig, T. Donner, and T. Esslinger, Rotom-type mode softening in a quantum gas with cavity-mediated long-range interactions, *Science* **336**, 1570 (2012).

[30] J. Klinder, H. Keßler, M. R. Bakhtiari, M. Thorwart, and A. Hemmerich, Observation of a Superradiant Mott Insulator in the Dicke-Hubbard Model, *Phys. Rev. Lett.* **115**, 230403 (2015).

[31] R. Landig, L. Hruby, N. Dogra, M. Landini, R. Mottl, T. Donner, and T. Esslinger, Quantum phases from competing short- and long- range interactions in an optical lattice, *Nature (London)* **532**, 476 (2016).

[32] S. F. Caballero-Benítez and I. B. Mekhov, Quantum Optical Lattices for Emergent Many-Body Phases of Ultra-

cold Atoms, Phys. Rev. Lett. **115**, 243604 (2015).

[33] S. F. Caballero-Benitez, G. Mazzucchi, and I. B. Mekhov, Quantum simulators based on the global collective light-matter interaction, Phys. Rev. A **93**, 063632 (2016).

[34] M. R. Bakhtiari, A. Hemmerich, H. Ritsch, and M. Thorwart, Nonequilibrium Phase Transition of Interacting Bosons in an Intra-Cavity Optical Lattice, Phys. Rev. Lett. **114**, 123601 (2015).

[35] Y. Chen, Z. Yu, and H. Zhai, Quantum phase transitions of the Bose-Hubbard model inside a cavity, Phys. Rev. A **93**, 041601(R) (2016).

[36] T. Flottat, L. de Forges de Parny, F. Hébert, V. G. Rousseau, and G. G. Batrouni, Phase diagram of bosons in a two-dimensional optical lattice with infinite-range cavity-mediated interactions, Phys. Rev. B **95**, 144501 (2017).

[37] W. Zheng and N. R. Cooper, Superradiance Induced Particle Flow via Dynamical Gauge Coupling, Phys. Rev. Lett. **117**, 175302 (2016).

[38] C. Kollath, A. Sheikhan, S. Wolff, and F. Brennecke, Ultracold Fermions in a Cavity-Induced Artificial Magnetic Field, Phys. Rev. Lett. **116**, 060401 (2016).

[39] K. E. Ballantine, B. L. Lev, and J. Keeling, Meissner-like Effect for a Synthetic Gauge Field in Multimode Cavity QED, Phys. Rev. Lett. **118**, 045302 (2017).

[40] B. Padhi and S. Ghosh, Spin-orbit-coupled Bose-Einstein condensates in a cavity: Route to magnetic phases through cavity transmission, Phys. Rev. A **90**, 023627 (2014).

[41] J.-S. Pan, X.-J. Liu, W. Zhang, W. Yi, and G.-C. Guo, Topological Superradiant States in a Degenerate Fermi Gas, Phys. Rev. Lett. **115**, 045303 (2015).

[42] F. Mivehvar, H. Ritsch, and F. Piazza, Superradiant Topological Peierls Insulator inside an Optical Cavity, Phys. Rev. Lett. **118**, 073602 (2017).

[43] C. Maschler, I. B. Mekhov, and H. Ritsch, Ultracold atoms in optical lattices generated by quantized light fields, Eur. Phys. J. D **46**, 545 (2008).

[44] S. Gopalakrishnan, B. L. Lev, and P. M. Goldbart, Emergent crystallinity and frustration with Bose-Einstein condensates in multimode cavities, Nat. Phys. **5**, 845 (2009).

[45] P. Domokos and H. Ritsch, Collective Cooling and Self-Organization of Atoms in a Cavity, Phys. Rev. Lett. **89**, 253003 (2002).

[46] D. Nagy, G. Szirmai, and P. Domokos, Critical exponent of a quantum-noise-driven phase transition: The open-system Dicke model, Phys. Rev. A **84**, 043637 (2011).

[47] J. Keeling, M. J. Bhaseen, and B. D. Simons, Fermionic Superradiance in a Transversely Pumped Optical Cavity, Phys. Rev. Lett. **112**, 143002 (2014).

[48] F. Dimer, B. Estienne, A. S. Parkins, and H. J. Carmichael, Proposed realization of the Dicke-model quantum phase transition in an optical cavity QED system, Phys. Rev. A **75**, 013804 (2007).

[49] J. Keeling, M. J. Bhaseen, and B. D. Simons, Collective Dynamics of Bose-Einstein Condensates in Optical Cavities, Phys. Rev. Lett. **105**, 043001 (2010).

[50] D. Nagy, G. Konya, G. Szirmai, and P. Domokos, Dicke-Model Phase Transition in the Quantum Motion of a Bose-Einstein Condensate in an Optical Cavity, Phys. Rev. Lett. **104**, 130401 (2010).

[51] D. Nagy, G. Szirmai, and P. Domokos, Self-organization of a Bose-Einstein condensate in an optical cavity, Eur. Phys. J. D **48**, 127 (2008).

[52] P. Horak and H. Ritsch, Dissipative dynamics of Bose condensates in optical cavities, Phys. Rev. A **63**, 023603 (2003).

[53] I. B. Mekhov, C. Maschler, and H. Ritsch, Cavity-Enhanced Light Scattering in Optical Lattices to Probe Atomic Quantum Statistics, Phys. Rev. Lett. **98**, 100402 (2007).

[54] I. B. Mekhov and H. Ritsch, Quantum Nondemolition Measurements and State Preparation in Quantum Gases by Light Detection, Phys. Rev. Lett. **102**, 020403 (2009).

[55] R. Landig, F. Brennecke, R. Mottl, T. Donner, and T. Esslinger, Measuring the dynamic structure factor of a quantum gas undergoing a structural phase transition, Nat. Commun. **6**, 7046 (2015).

[56] N. Dogra, M. Landini, K. Kroeger, L. Hruby, T. Donner, and T. Esslinger, Dissipation-induced structural instability and chiral dynamics in a quantum gas, Science **366**, 1496 (2019).

[57] R. M. Kroeze, Y. Guo, V. D. Vaidya, J. Keeling, and B. L. Lev, Spinor Self-Ordering of a Quantum Gas in a Cavity, Phys. Rev. Lett. **121**, 163601 (2018).

[58] L. Hruby, N. Dogra, M. Landini, T. Donner, and T. Esslinger, Metastability and avalanche dynamics in strongly-correlated gases with long-range interactions, Proc. Natl. Acad. Sci. U.S.A. **115**, 3279 (2018).

[59] K. Kroeger, N. Dogra, R. Rosa-Medina, M. Paluch, F. Ferri, T. Donner, and T. Esslinger, Continuous feedback on a quantum gas coupled to an optical cavity, New J. Phys. **22**, 033020 (2020).

[60] Y. Guo, V. D. Vaidya, R. M. Kroeze, R. A. Lunney, B. L. Lev, and J. Keeling, Emergent and broken symmetries of atomic self-organization arising from Gouy phase shifts in multimode cavity QED, Phys. Rev. A **99**, 053818 (2019).

[61] Y. Guo, R. M. Kroeze, V. D. Vaidya, J. Keeling, and B. L. Lev, Sign-Changing Photon-Mediated Atom Interactions in Multimode Cavity Quantum Electrodynamics, Phys. Rev. Lett. **122**, 193601 (2019).

[62] V. D. Vaidya, Y. Guo, R. M. Kroeze, K. E. Ballantine, A. J. Kollár, J. Keeling, and B. L. Lev, Tunable-Range, Photon-Mediated Atomic Interactions in Multimode Cavity QED, Phys. Rev. X **8**, 011002 (2018).

[63] R. M. Kroeze, Y. Guo, and B. L. Lev, Dynamical Spin-Orbit Coupling of a Quantum Gas, Phys. Rev. Lett. **123**, 160404 (2019).

[64] P. Zupancic, D. Dreon, X. Li, A. Baumgärtner, A. Morales, W. Zheng, N. R. Cooper, T. Esslinger, and T. Donner, *P*-Band Induced Self-Organization and Dynamics with Repulsively Driven Ultracold Atoms in an Optical Cavity, Phys. Rev. Lett. **123**, 233601 (2019).

[65] A. Morales, D. Dreon, X. Li, A. Baumgärtner, P. Zupancic, T. Donner, and T. Esslinger, Two-mode Dicke model from nondegenerate polarization modes, Phys. Rev. A **100**, 013816 (2019).

[66] Z. Zhang, C. H. Lee, R. Kumar, K. J. Arnold, S. J. Mason, A. S. Parkins, and M. D. Barrett, Nonequilibrium phase transition in a spin-1 Dicke model, Optica **4**, 424 (2017).

[67] J. Fan, X. Zhou, W. Zheng, W. Yi, G. Chen, and S. Jia, Magnetic order in a Fermi gas induced by cavity-field fluctuations, Phys. Rev. A **98**, 043613 (2018).

[68] F. Mivehvar, S. Ostermann, F. Piazza, and H. Ritsch, Driven-Dissipative Supersolid in a Ring Cavity, Phys. Rev. Lett. **120**, 123601 (2018).

[69] F. Mivehvar, H. Ritsch, and F. Piazza, Emergent Qua-

sicrystalline Symmetry in Light-Induced Quantum Phase Transitions, Phys. Rev. Lett. **123**, 210604 (2019).

[70] K. Gietka, F. Mivehvar, and H. Ritsch, A supersolid-based gravimeter in a ring cavity, Phys. Rev. Lett. **122**, 190801 (2019).

[71] F. Mivehvar, H. Ritsch, and F. Piazza, Cavity-quantum-electrodynamical toolbox for quantum magnetism, Phys. Rev. Lett. **122**, 113603 (2019).

[72] C.-M. Halati, A. Sheikhan, H. Ritsch, and C. Kollath, Dissipative generation of highly entangled states of light and matter, arXiv: 1909.07335 (2019).

[73] C. Rylands, Y. Guo, B. L. Lev, J. Keeling, and V. Galitski, Photon-mediated Peierls Transition of a 1D Gas in a Multimode Optical Cavity, arXiv: 2002.12285 (2020).

[74] S. Ostermann, W. Niedenzu, and H. Ritsch, Unraveling the quantum nature of atomic self-ordering in a ring cavity, Phys. Rev. Lett. **124**, 033601 (2020).

[75] P. Nataf, A. Baksic, and C. Ciuti, Double symmetry breaking and two-dimensional quantum phase diagram in spin-boson systems, Phys. Rev. A **86**, 013832 (2012).

[76] A. Baksic and C. Ciuti, Controlling Discrete and Continuous Symmetries in “Superradiant” Phase Transitions with Circuit QED Systems, Phys. Rev. Lett. **112**, 173601 (2014).

[77] M. Landini, N. Dogra, K. Kröger, L. Hruby, T. Donner, and T. Esslinger, Formation of a Spin Texture in a Quantum Gas Coupled to a Cavity, Phys. Rev. Lett. **120**, 223602 (2018).

[78] E. I. Rodríguez Chiacchio and A. Nunnenkamp, Dissipation-Induced Instabilities of a Spinor Bose-Einstein Condensate Inside an Optical Cavity, Phys. Rev. Lett. **122**, 193605 (2019).

[79] B. Buča and D. Jaksch, Dissipation Induced Nonstationarity in a Quantum Gas, Phys. Rev. Lett. **123**, 260401 (2019).

[80] M. Soriente, R. Chitra, and O. Zilberberg, Distinguishing phases using the dynamical response of driven-dissipative light-matter systems, Phys. Rev. A **101**, 023823 (2020).

[81] W. P. Schleich, *Quantum Optics in Phase Space* (Wiley, Berlin, 2001).

[82] A. Klein and E. R. Marshalek, Boson realizations of Lie algebras with applications to nulear physics, Rev. Mod. Phys. **63**, 375 (1991).

[83] T. Yoshino, Compact and Highly Efficient Faraday Rotators Using Relatively Low Verdet Constant Faraday Materials, Jpn. J. Appl. Phys. **19**, 745 (1980).

[84] H. M. Wiseman and G. J. Milburn, Quantum theory of field-quadrature measurements, Phys. Rev. A **47**, 642 (1993).

[85] A. Baksic, P. Nataf, and C. Ciuti, Superradiant phase transitions with three-level systems, Phys. Rev. A **87**, 023813 (2013).

[86] S. Cordero, R. López-Peña, O. Castaños, and E. Nahmad-Achar, Quantum phase transitions of three-level atoms interacting with a one-mode electromagnetic field, Phys. Rev. A **87**, 023805 (2013).